CHALMERS
UNIVERSITY OF TECHNOLOGY

ROAD PROFILE ESTIMATION AND CLASSIFICATION

Design of robust $\mathcal{H}_\infty$ observer for profile estimation and classification based on the ride comfort

Master's thesis in Systems, Control and Mechatronics

SACHIN MADHUSUDHANA

Road Profile Estimation and Classification

Design of robust $\mathcal{H}_\infty$ observer for profile estimation and classification based on the ride comfort

SACHIN MADHUSUDHANA

Road profile estimation and classification
Design of robust $\mathcal{H}_\infty$ observer for profile estimation and classification based on the ride comfort
Sachin Madhusudhana

Sachin Madhushadhana
Systems, Control and Mechatronics
Chalmers University of Technology

ABSTRACT

The current active suspension systems are tuned extensively on different types of roads to have a good vehicle comfort and handling for safety and economic savings. Even though different modes can be chosen depending on the mode of the driver, such as comfort or dynamic, no adaptation of these modes are made for different road surfaces. The knowledge of the road profile estimation can be used to adapt the damping coefficient on active or semi-active suspension control systems to improve the ride comfort and handling of a car. Recent improvement in communication has enabled advancement in approaches towards vehicle safety which makes it possible for communication between the road infrastructure and the vehicle.

This master thesis involves the implementation of a road profile estimation method with the measurements obtained from the sensors placed in the vehicle. The suspension variables used in the estimation method is obtained from a robust $\mathcal{H}_\infty$observer by modelling a quarter car vertical model. The robust observer is a frequency dependant optimization framework providing better results of estimation in an uncertain and noisy environment. Frequency weightings is formulated in the state space form which prevents the cancellation of important dynamics of the system. The road irregularities are further validated using Fourier analysis providing information about the frequency components of the estimated profiles. One type of information that is important to distinguish is the amplitude versus wavelength spectra of the road. The road classification is done on the basis of ISO8608 standards and extended for inclusion of more harmonic components along the road profile.

Power Spectral Density(PSD) gives the best idea for the determining the road roughness and a standard for the classification of the road. Furthermore this classified road data is stored in a cloud service, which provides an online infrastructure communicating with vehicle about the road surface ahead. Finally this opens a new dimension to tune the controller adaptively to optimize the comfort and handling of the vehicle on any stretch of road.

Keywords: PSD, $\mathcal{H}_\infty$observer, Fourier analysis, Road profile, Semi-active suspension, ISO8608, quarter car model

Acknowledgements

x

x

Contents

List of Figures

List of Tables

1

Introduction

1.1 Motivation

In today's world we have highest number of vehicles on road, and this number seems to ever increase with the advancement in technologies in the automotive industry with autonomous vehicles and electro-mobility. Vehicle dynamics is a major area with continuous development in the handling and comfort of the vehicle. One such important factor which is the primary input to the vehicle is the road profile which determines the vehicle performance.This information is used to adapt different suspension features. The estimated road profile is used to adaptively change the damping coefficient in the semi-active or the active suspensions control to tweak the handling and the stability of the car.

A bad road might cause severe damage to the vehicle components at different frequencies, which results in increase in the operational costs when there is a damage. According to the report [1] the road expenses is about 20 billion Euros in EU each year and in Germany is said to reach from 2.7 billion Euros in 2015 to 3.6 billion Euros in 2025 [2]. Hence such a method is necessary to estimate the road profile beforehand. The federal highway administration (FHA) under U.S development of transportation started the long term pavement performance (LTTP) in 1987 [3]. It has standard data collection procedures divided into two sets namely general pavement studies (GPS) and specific pavement studies (SPS), where GPS is for existing profiles and SPS included ten levels built for specific designs of the road. This motivates for a lot of research on the importance of the road profile information. A route planning algorithm is proposed [4] based on the passenger feeling, improving overall time and ride comfort. [5] proposed a precision enhancement of pavement roughness localization among the connected vehicles. The semi-active suspensions present in the current market assume the road conditions to be unknown because the relation between to the ride comfort and the handling are difficult to be satisfied simultaneously [6].

Therefore an adaptive estimation is important for commercial applications of semi-active suspension systems. Another scope of the thesis is to have a preview knowledge of the road for control of the dampers through a cloud based service. This provides an important bandwidth of the road profile as it is a primary input of vehicle dynamics for control of handling and comfort.

1.2 Road Profile Estimation Overview

The road estimation has attracted major interest between the automotive manufacturers and government in recent decades[23]. There are different methods to classify roads which are:

1.2.1 Direct Measurement

Currently the adopted standards to determine the road profile uses a specially designed device which comes in contact with the road irregularities. These devices are called as profilometers or profilographs [7]. The accuracy of the estimation is very high in this case. However, this is really expensive and can be affected by adverse change in the environment. Two examples of the equipment used for the estimations are:

- Dipstick profiler : A dipstick profiler consists of an inclinometer with two legs collecting relatively very small quantity of road profile measurements. It has two digital displays on the end of both the legs to provide relative elevation between them. This method requires a person to walk through the elevation in the pavement profile by pivoting around each leg of the profiler.These instruments usually have accuracy around 0.1mm and sometimes used in calibration of more sophisticated profilers.
- Profilographs : A profilograph is mounted with a sensing wheel to provide free vertical movement at the center frame to determine the undulations from the road roughness. The recorded profile is then obtained in a graph. They have a different structure to that of the dipstick profiler and data processing methods. The accuracy of such is around 100mm with a range from 0.05cycles/m to 2 cycles/m [8].

1.2.2 Non-contact Measurement

There are several existing methods that uses visual inspections to determine the road depths through either camera or depth sensors.These generally are non contact sensors like lasers and infrared transceivers mounted on the vehicle to determine the distance between the light from the lasers and the road surface. In current commercialized laser displacement sensors for road profilometry it is possible to measure the road surfaces for upto 200mm with accuracy of 1% of the measurement range [9]. Similar concepts can be seen which is based on the non contact measurement [11, 12].

1.2.3 Indirect Measurement

An alternative method used is the response based system. With advancement of technologies and stricter rules for the automotive industries, it has led to increase in the sensors used in the vehicles. This is an indirect method that uses the information from the sensors equipped in the vehicle such as the suspension deflection sensors

and the accelerometers. An observer based techniques are used to determine the road conditions. The generated road profiles in time domain can be used to modify controller parameter gains [10] . Many different methods are proposed for road profile estimation.

Hrovat et al[13] proposes rattle space deflection to determine road conditions. Frequency based estimation using sprung mass accelerations was proposed by Yi et al [14]. A sliding mode observer was proposed by comparing it with a profilograph [15]. Doumiati et al [16] used Kalman filter to determine road excitation in real time. Time domain estimation for semi-active suspension systems using Youla parametrization was proposed by Martinez et.al [17].

The response based systems are classified into two categories:
- Road profile estimation in time domain
- Road level classification

The profile estimation uses observer based models to reconstruct the road irregularities. These models uses inverse based modelling with no prior knowledge of the road surface profile. Whereas road classification refers to algorithms to determine the level of the road excitation estimated.

A transfer function based approach road classification using just the measurement of the unsprung mass accelerations was proposed by [24]. It was then extended by Wang et al [18] to include varying velocities and experimental validation was done to validate the algorithm. A speed independent road classification algorithm was proposed by Qin et al [19] without any prior information of the road profile. The results showed the robustness towards the change in the parameters and vehicle velocity. With greater development in the fields of the Machine learning there are many papers which uses neural networks to classify roads. Ngwangwa et al [20] uses Back propagation and neural networks to classify road irregularities.

For time domain profile estimation Kang et al. used a discrete Kalman filter with unknown road input and compared the results with laser profilometer form a test vehicle [21]. Wang et al. combined a model error with Kalman filter and used simulation results to validate with the proposed algorithm [22].
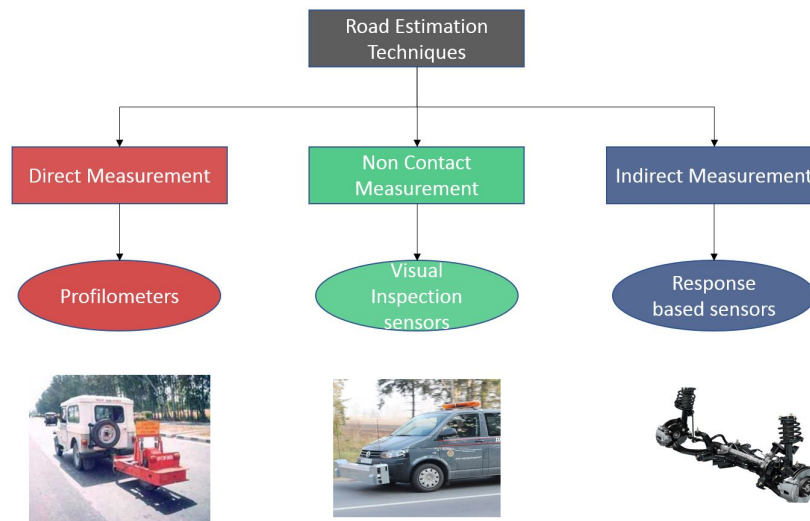
Figure 1.1: Different road estimation models

Figure 1.1 represents the different ways of classifying roads as discussed above. The scope in this thesis makes use of the response based systems where the sensors used for measurements are sprung mass accelerations and unsprung mass accelerations.

1.3   Summary

A literature review of different estimation methods were presented. The growing importance in road safety and interest in research of different methods for estimation and classification is shown. The current methods to estimate the road profile include direct measurement, non contact measurement and indirect measurement. The indirect measurement i.e response based measurement are the best among the three categories since they provide marginal accuracy with lower cost. Therefore a system based on the indirect measurement for road profile estimation is built in this thesis.

2

Theory

2.1 Vehicle Modeling

Vehicle system models are presented in this chapter. Vertical dynamics of the vehicle is considered to model the system since the impact of a road input on the vehicle is vertical. The major part of the vertical dynamics includes the automotive suspension systems which rests the vehicle body on its axles. Modeling can be done with a 7 degree full car vertical model, or a 4 degree half car model or a 2 degree quarter car model. A quarter car model represents a suspension system at each wheels of the vehicle. Some of the functions of this system is to isolate the vehicle body from the external road disturbance to give good ride quality, to provide good handling and support the vehicle's static weight. We will consider two systems on to which the damper settings can be controlled i.e. active and semi-active suspension systems.

2.1.1 Active Suspensions

The passive suspension systems have significant trade-offs between ride quality and suspension deflection. Improvements in one of the factors will deteriorate other factor. The active suspension uses electronically controlled dampers to provide superior ride quality.It offers more refined riding experience. An active suspension system has the ability to store, dissipate and introduce energy into the system. These systems help in effectively reduce the body roll,pitch and heave. Though a fully active system will consume more power than semi-active suspension systems.

2.1.2 Semi-Active Suspensions

A semi active suspension system in the vehicle uses a variable damper by controlling the damper force based on the continuously varying road surface, where the road surface is not measured directly. It is similar to active suspension systems but with an adjustable shock absorber. A semi active suspension model can be employed by several control strategies, where the most common control strategy still used is a skyhook controller. An example of a semi-active suspension is a magneto rheological (MR) damper. The MR damper uses an MR fluid which reacts to changes in the magnetic field. The dissipative force for the damper can be obtained by varying the electromagnetic field to cause an effect in the movement of the fluid in the container. Another type of semi-active dampers

The semi active suspension use less power when compared to active suspension systems. Here the power is used only to change the electromagnetic field using the

current through the coil in the MR damper. No external power is used unlike the active systems to counter the vibratory forces. In case of the semi-active dampers with control valves, the damping force depends on the piston speed, the damping force is directly proportional to the piston speed. The degree by which the piston motion moves is controlled by the valves. This thesis will make use of semi active suspensions with internal valves, but can also be used with the passive dampers as long as the damping force is characterized.

2.1.2.1 CCD Model

The CCD damper model can be continuously adjusted according to the ride modes required and continuous information regarding the body and wheel motion in the vehicle. The dissipative force obtained from this model is a function of the deflecting velocity. At different values of current different forces can be obtained. A damper model characteristic is usually non-linear as seen in figure 2.1.The effective damping must be lowered for high velocities to minimize the transmissibility of the disturbances to the passengers. Similarly lower velocities the damping should be larger. Having higher damping is not necessary during compression as additional energy will get stored in the springs. Therefore lower damping is given for positive velocities since the springs will resist any further compression. But is not the case in negative velocities as it will further increase the effective damping.
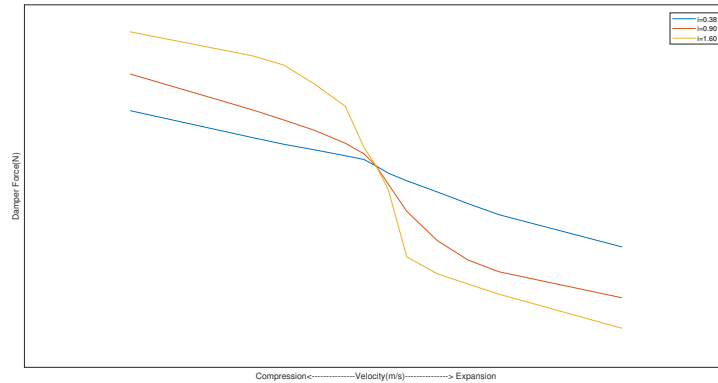
Figure 2.1: CCD damper force from deflecting velocity

2.1.3 Quarter Car Modeling

One of the most used vertical model for the study of vehicle suspension is the quarter car model shown in figure 2.2. The vertical model uses two solid suspended masses denoted as sprung mass m_s and unsprung mass m_{us}. The sprung mass denotes $\frac{1}{4}^{th}$ of the body of the vehicle and the unsprung mass represents the mass of the wheel and the components connected to it. The spring is considered to be linear because the application it has in automotive applications is almost 95% in linear region. The spring stiffness coefficient of the spring k_s and that of the wheel k_t. The damping

coefficient is b_s.
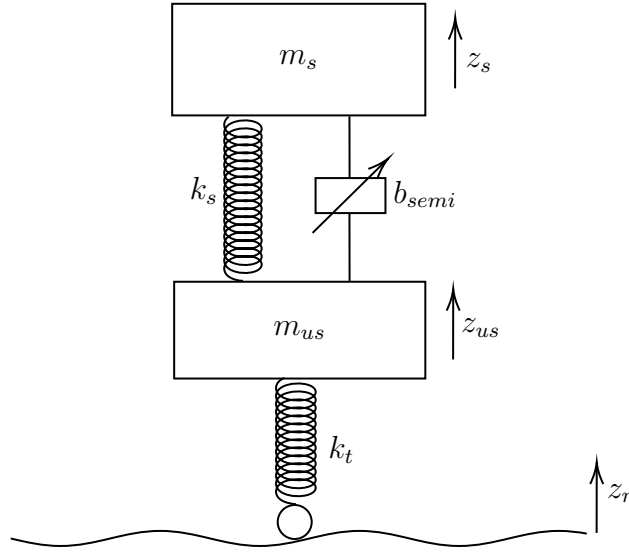
Figure 2.2: Quarter Car Model

The dynamics of motion governing the two degree of freedom vertical model is given by

$$m_s\ddot{z}_s(t) + b_{semi}(t)(\dot{z}_s(t) - \dot{z}_{us}(t)) + k_s(z_s(t) - z_{us}(t)) = 0$$
$$m_{us}\ddot{z}_u s(t) - b_{semi}(t)(\dot{z}_s(t) - \dot{z}_{us}(t)) + k_t(z_{us}(t) - z_r(t)) - k_s(z_s(t) - z_{us}(t)) = 0$$
$$(2.1)$$

Here, $b_{semi}(t)(z_s(t) - z_{us}(t))$ is considered to be the variable damper force F_d to adjust the handling or comfort. Therefore the dynamics can be re-written as

$$m_s\ddot{z}_s(t) + k_s(z_s(t) - z_{us}(t)) = -F_d(t)$$
$$m_{us}\ddot{z}_u s(t) + k_t(z_{us}(t) - z_r(t)) - k_s(z_s(t) - z_{us}(t)) = F_d(t)$$
$$(2.2)$$

The state space model of the quarter car model for the semi active suspension model can be written as:

$$\dot{x}(t) = Ax(t) + Bu(t) + Lz_r(t) \qquad (2.3)$$

States of the model are considered to be

$x_1(t) = z_s(t)$ Sprung mass displacement
$x_2(t) = \dot{z}_s(t)$ Sprung mass velocity
$x_3(t) = z_{us}(t)$ Unsprung mass displacement
$x_4(t) = \dot{z}_{us}(t)$ Unsprung mass velocity

And, inputs
$u(t) = F_d(t)$ Damper Force
$z_r(t)$ Road profile

State space representation of the model is given by

$$\dot{x}(t) = \begin{bmatrix} \dot{z}_s(t) \\ \ddot{z}_s(t) \\ \dot{z}_{us}(t) \\ \ddot{z}_{us}(t) \end{bmatrix} \tag{2.4}$$

$$\dot{x}(t) = \begin{bmatrix} 0 & 1 & 0 & 0 \\ -k_s/m_s & 0 & k_s/m_s & 0 \\ 0 & 0 & 0 & 1 \\ k_s/m_{us} & 0 & -(k_s+k_t)/m_{us} & 0 \end{bmatrix} \begin{bmatrix} z_s(t) \\ \dot{z}_s(t) \\ z_{us}(t) \\ \dot{z}_{us}(t) \end{bmatrix} + \begin{bmatrix} 0 & 0 \\ 1/m_s & 0 \\ 0 & 0 \\ -1/m_{us} & k_t/m_{us} \end{bmatrix} \begin{bmatrix} u(t) \\ z_r(t) \end{bmatrix} \tag{2.5}$$

$$\begin{bmatrix} y_1(t) \\ y_2(t) \end{bmatrix} = \begin{bmatrix} 1 & 0 & -1 & 0 \\ -k_s/m_s & 0 & k_s/m_s & 0 \end{bmatrix} \begin{bmatrix} z_s(t) \\ \dot{z}_s(t) \\ z_{us}(t) \\ \dot{z}_{us}(t) \end{bmatrix} + \begin{bmatrix} 0 & 0 \\ 1/m_s & 0 \end{bmatrix} \begin{bmatrix} u(t) \\ z_r(t) \end{bmatrix} + \begin{bmatrix} n_1(t) \\ n_2(t) \end{bmatrix} \tag{2.6}$$

Where y_1 and y_2 are the observed data with n_1 and n_2 are the corresponding noises from the sensor modules. The parameters used in designing the model is given in table 2.1

m_s	608.7
m_{us}	52.611
k_s	45356.3
k_t	286882

Table 2.1: Vehicle Parameters

The states that are used to determine the vehicle performance in the vertical dynamics are hard to obtain. Hence a $\mathcal{H}_\infty$ observer is designed to estimate the the states and handle the uncertainties and disturbances.

2.1.3.1 Observability Analysis

This analysis is used to determine how well the internal states are easy to deduce based on the system input and output. Since the system designed above is a linear system, the observability condition can be checked by Kalman test

$$\mathcal{O} = \begin{bmatrix} C & CA & CA^2 & CA^3 \end{bmatrix} \tag{2.7}$$

For the system to be observable the rank of the matrix must be equal to the number of states of the system i.e $rank(\mathcal{O}) = n$. For the above system the observability condition holds true.

2.1.3.2 Model Validation

In control applications all the types of model needs to be validated to ensure that the region around which it is operated should be very similar to that of the non-linear model. Therefore it is necessary that the model is applicable for the designed operation. Hence, the output of the linear models should match that of the non-linear model in the respective time domain.

To test the linear model, the vehicle is run on two road profiles A and B in the Carmaker. The algorithm is written in Matlab, where the linear model is built. It is possible to collect data from Carmaker to Simulink. Results for which can be seen in figures 2.3 and 2.4. The model outputs are in red color whereas the Carmaker model is in blue color. The four states match that of the non linear model. The similar roads A and B will be used for the analysis of observer.
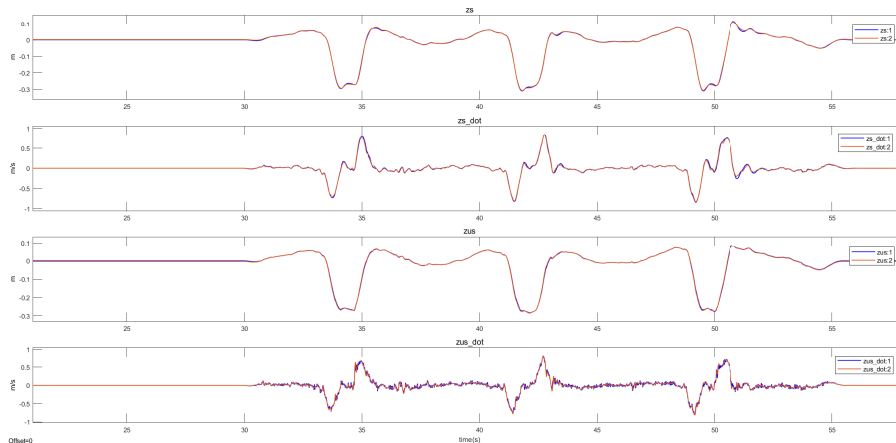

Figure 2.3: Suspension variables on road profile A
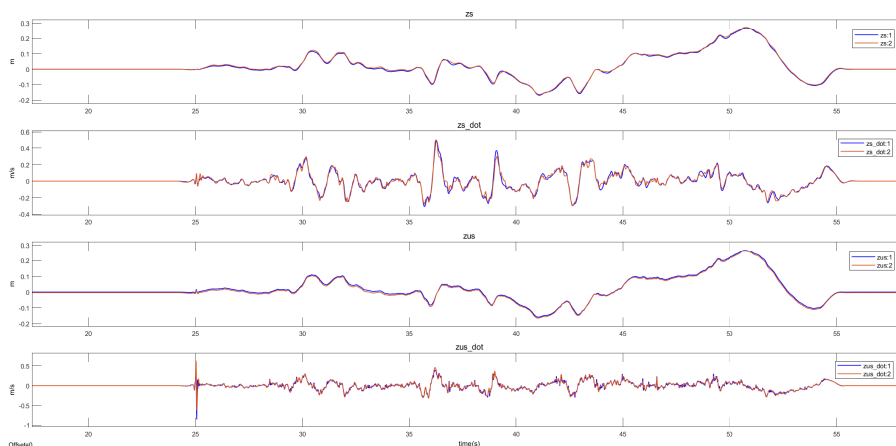
Figure 2.4: Suspension variables on road profile B

2.2 Road Profile Estimation and Modeling

The standard definition of road profile is the distance between the road surface and the base of the measuring device in a contact based instruments. Unsprung mass accelerations measurements are close to determination of the road profile $z_r(t)$. By using the estimated states from the observer, it is possible to determine the road profile from the static equation of the unsprung mass acceleration

$$\hat{z}_r(t) = (m_{us}\ddot{\hat{z}}_{us}(t) - k_s(\hat{z}_s(t) - \hat{z}_{us}(t)) + k_t\hat{z}_{us}(t) + F_d(t))/k_t \tag{2.8}$$

Since the measurement that is used from the sprung mass accelerations $(\ddot{z}_s)$ and suspension deflection alone, the unsprung mass accelerations $\ddot{\hat{z}}_{us}$ is estimated. F_d is the damper force that is obtained form the CCD model.

The statistical characteristics of such road surfaces based on amplitude and frequency can be used to classify the type of road. Power spectral densities is one such way to give a better understanding of the road irregularities.

2.3 Observer Design

A general structure of an observer to estimate the unobservable states is shown in figure 2.5, where the measurements are the input to an observer which estimate the states based on an estimation algorithm. The error term that is obtained as result of difference between true states and the observer output has to be reduced. There are many such observer structures for state estimation. In this thesis $\mathcal{H}_\infty$ observer is the one chosen.
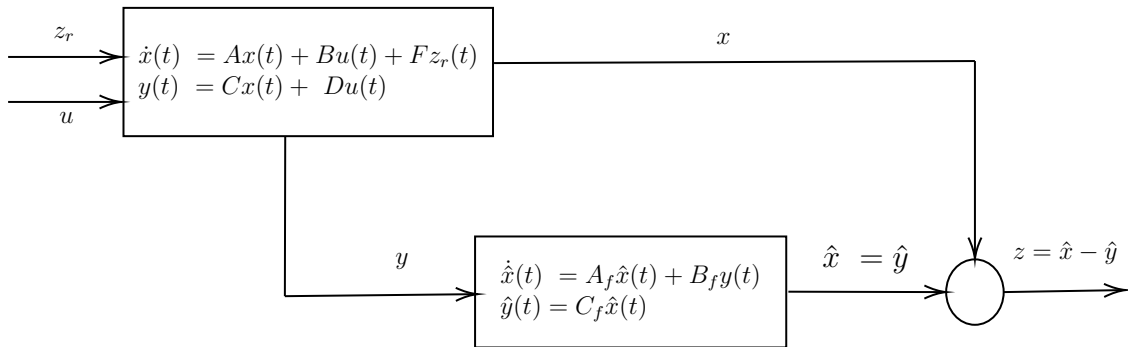
Figure 2.5: General observer structure

The $\mathcal{H}_\infty$ observer is a Luenberger state observer which is an extension of $\mathcal{H}_\infty$ controller optimization framework. Therefore, a linearised search algorithm for the $\mathcal{H}_\infty$ can be straight forwardly applied to this problem.

The general LTI plant used for the synthesis of $\mathcal{H}_\infty$ observer is given by

$$P = \begin{cases} \dot{x}(t) = Ax(t) + Bu(t) + Fz_r(t) \\ y(t) = Cx(t) + Du(t) \\ z(t) = W_{ei}(t)(x(t) - \hat{x}_i(t)) \end{cases} \tag{2.9}$$

where $x(t)$ is the states, $u(t)$ is the control input and $z_r(t)$ is the unknown road input to the system. $y(t)$ is the measured outputs and $z(t)$ is the performance outputs. W_{ei} is the performance dynamic weightings on the states for error minimization.

An augmented model for the quarter car system is built for this observer design to establish the disturbance rejection and reduce integration drift in the states. The updated measurement equation of which along with the performance outputs as mentioned in 2.9 is augmented as

$$y(t) = \underbrace{\begin{bmatrix} 1 & 0 & 0 & 0 \\ 0 & 1 & 0 & 0 \\ 0 & 0 & 1 & 0 \\ 0 & 0 & 0 & 1 \\ 0 & 1 & 0 & -1 \\ 1 & 0 & -1 & 0 \\ -k_s/m_s & 0 & k_s/m_s & 0 \end{bmatrix}}_{C_2} \begin{bmatrix} z_s(t) \\ \dot{z}_s(t) \\ z_{us}(t) \\ \dot{z}_{us}(t) \end{bmatrix} + \underbrace{\begin{bmatrix} 0 & 0 \\ 0 & 0 \\ 0 & 0 \\ 0 & 0 \\ 0 & 0 \\ 0 & 0 \\ 1/m_s & 0 \end{bmatrix}}_{D_2} \begin{bmatrix} u(t) \\ z_r(t) \end{bmatrix} \qquad (2.10)$$

The augmented plant model now consists of the measured outputs and performance outputs useful for the observer synthesis. The observer dynamics is given by $\dot{\hat{x}} = A_f \hat{x}(t) + B_f y(t)$, which is quadratically stable.

Figure 2.6: Closed loop observer structure

With reference to general controller configuration in 2.6, the central controller has same number of states as the generalized plant P. Therefore the central controller can be divided into state observer and a state feedback control. For this thesis requires just the design of state observer. The general algorithm for the $\mathcal{H}_\infty$ synthesis
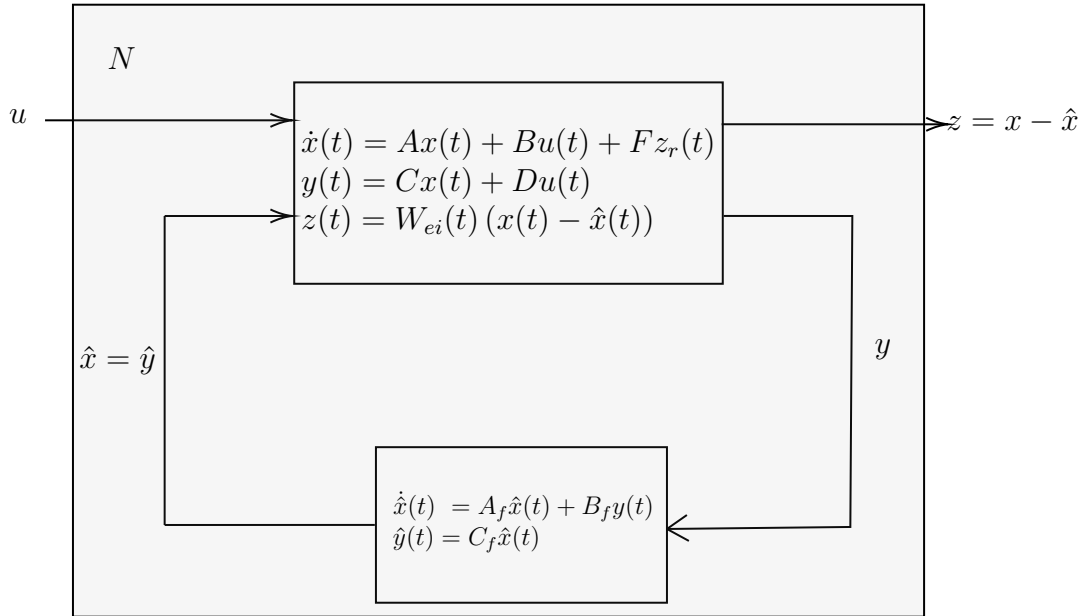
is given by a law satisfying the optimal law $||F_l(P, K)||_\infty < \gamma$ where γ is the performance level and F_l is the lower fractional transformation i.e the interconnection between the plant and the controller ($N = F_l(P, K)$). K is a stabilizing controller if and only if,

(i) $X_\infty > 0$ is a solution to riccati equation

$$A^T X_\infty + X_\infty A + C_1^T C_1 + X_\infty (\gamma^{-2} B_1 B_1^T - B_2 B_2^T) X_\infty = 0 \qquad (2.11)$$

such that Re $\lambda_i[A + (\gamma^{-2} B_1 B_1^T - B_2 B_2^T) X_\infty] < 0$, $\forall i$, and

(ii) $Y_\infty > 0$ is a solution to riccati equation

$$A^T Y_\infty + Y_\infty A + B_1^T B_1 + Y_\infty (\gamma^{-2} C_1 C_1^T - C_2 C_2^T) Y_\infty = 0 \qquad (2.12)$$

such that Re $\lambda_i[A + ((\gamma^{-2} C_1 C_1^T - C_2 C_2^T) Y_\infty]$, $\forall i$, and

(iii) $\rho(X_\infty Y_\infty) < \gamma^2$

Such controllers are given by $K = F_l(K_c, Q)$ where

$$K_c(s) = \mathcal{L} \left[\begin{array}{c|cc} A_\infty & -Z_\infty\, L_\infty & Z_\infty\, B_\infty \\ \hline F_\infty & 0 & I \\ -C_2 & I & 0 \end{array} \right]$$

$$F_\infty = -B_2^T X_\infty, \;\; L_\infty = -Y_\infty C_2^T, \;\; Z_\infty = (I - \gamma^{-2} Y_\infty X_\infty)^{-1} \qquad (2.13)$$

$$A_\infty = A + \gamma^{-2} B_1 B_1^T X_\infty + B_2 F_\infty + Z_\infty L_\infty C_2 \qquad (2.14)$$

where Q(s) is a stable transfer function, such that $||Q||_\infty < \gamma$ and $\mathcal{L}$ is the Laplace transform.

If $Q(s) = 0$ then

$$K(s) = K_{c_{11}}(s) = -Z_\infty L_\infty (sI - A_\infty)^{-1} F\infty \qquad (2.15)$$

we obtain the central controller. As explained in the beginning a central controller has same number as the plant model and can be separated into a state observer

$$\dot{\hat{x}}(t) = A\hat{x}(t) + B_1 \underbrace{\gamma^{-2} B_1^T X_\infty(t)\hat{x}}_{worst\ case} + B_2 u(t) + Z_\infty L_\infty (C_2 \hat{x}(t) - y(t)) \qquad (2.16)$$

and a state feedback

$$u(t) = F_\infty \hat{x}(t) \qquad (2.17)$$

The worst case disturbance is an exogenous input to the system as shown in 2.16. The $\mathcal{H}_\infty$ algorithm is carried out generally by using the Matlab toolboxes. This allows to have a γ iteration to determine the best performance of the observer.

This $\mathcal{H}_\infty$ optimization technique is used to shape the singular values of the weighting function over a desirable bandwidth by minimizing energy in the error signals included by the uncertainty, noise and other disturbances. The difficult part of the optimization technique is the choice of the weighting function i.e to choose a good trade off at conflicting objectives in frequency ranges, which is described in the section 3

2.3.1 μ synthesis with DK-iteration

In general, two observer design is possible to achieve robustness to error $\mathcal{H}_\infty$ synthesis along with μ synthesis, of which $\mathcal{H}_\infty$ is already studied in the previous section. The main difference is, the $\mathcal{H}_\infty$ deals with minimizing the uncertainty in the plant. If the uncertainty in the plant is unstructured then it means that the uncertainty in the plant couples with each other. For example, in case of the mass damper system of the suspension the uncertainty in the mass does not couple with that of the spring constant, but $\mathcal{H}_\infty$ assumes so. Whereas μ synthesis assumes structured uncertainty where the actuator uncertainty as considered in this observer design does not couple with suspension parameters. The structured value of μ is a powerful tool for robust performance analysis. DK-iteration is one such technique that is used to synthesize the observer which combines $\mathcal{H}_\infty$ and μ synthesis to get good results.

The DK method applies upper bound on the μ in terms of scaled singular value

$$\mu(N) \leq \min_{D \epsilon D_s} \bar{\sigma}(DND^{-1}) \tag{2.18}$$

where N is the interconnection matrix of the closed loop and D, the dynamic weight is the applied upper bound. D_s is the domain of the stable weighting.

This operation minimizes the peak over frequency of this upper bound, such as

$$\min_K (\min_{D \epsilon D} ||(DN(K)D^{-1}||_\infty) \tag{2.19}$$

The DK-iteration process happens as follows:

- **K-step**: $\mathcal{H}_\infty$ synthesis for the scaled problem with a constant D $\min_K ||(DN(K)D^{-1}||_\infty$

- **D-step**: Finding D(jw) to minimise at each frequency $\sigma(DN\bar{D}^-1(jw))$ with fixed N.

The iteration continues until a satisfactory result is obtained $||(DN(K)D^{-1}||_\infty < 1$ or until the norm will no longer decrease. Matlab uses function called *dksyn* to perform this iteration and give the best μ value.

One such example can be seen in figure 2.7, which shows the difference between the $\mathcal{H}_\infty$ synthesis and μ synthesis. It is clear to see that μ sythensis gives the best performance to uncertainties and errors in the systems.
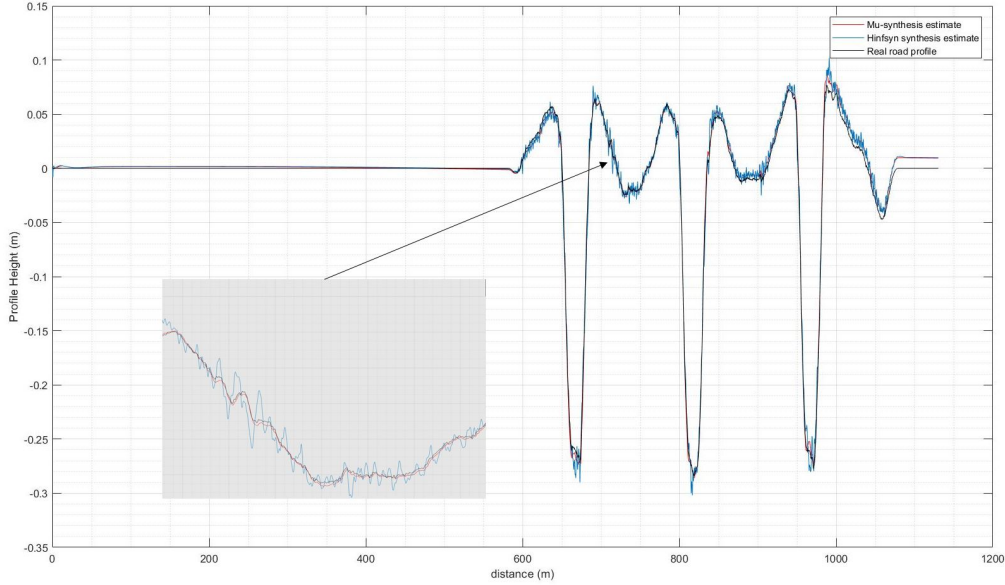

Figure 2.7: Difference in the observer synthesis

2.4 Frequency Analysis and PSD

A road profile is a collection of many different periodic sinusoidal signals, which contains many frequency irregularities. This thesis aims to classify the roads in terms of spectral densities. The power spectral density(PSD) is the magnitude squared of the Fourier transform of a continuous time and finite power signal. The PSD describes the amount of power present in each frequencies unlike the energy spectral densities which is suitable only for transient signals where energy is concentrated only in a single time window. For signals such as continuous time signals such as stationary process PSD is defined.

In general the average power of a signal say $x(t)$ over a time period is given by

$$P_x = \lim_{T \mapsto \infty} \frac{1}{T} \int_0^T |x(t)|^2 dt \tag{2.20}$$

To get the frequency component of the signal a Fourier transform has to be applied over the time period [0,T] as mentioned above.

$$\hat{x}(w) = \frac{1}{\sqrt{T}} \int_0^T x(t)e^{-jwt} dt \tag{2.21}$$

shows the amplitude spectral density of the signal.

And the power spectral density is given by

$$S_{xx} = \lim_{T \mapsto \infty} \mathbf{E}[|\hat{x}(w)|^2] \tag{2.22}$$

where, $\mathbf{E}$ is the expected value given by the Fourier transform

$$\mathbf{E}[|\hat{x}(w)|^2] = \frac{1}{T} \int_0^T \int_0^T \mathbf{E}[x^*(t)x(t')]e^{-jw(t-t')}dtdt' \tag{2.23}$$

Eqn 2.23 represents the auto-correlation function of the signal $x(t)$

$$R_{xx}(\tau) = (X(t)^*X(t+\tau)) \tag{2.24}$$

PSD is defined by the auto-correlation function by

$$S_{xx} = \int_0^T R_{xx}(\tau)e^{-jw\tau}d\tau = \hat{R}_{xx}(w) \tag{2.25}$$

provided $R_{xx}(\tau)$ is integrable.

3
Methodology

3.1 Model Based Estimation Algorithm

The design methodology implemented in this thesis is shown in figure 3.1.
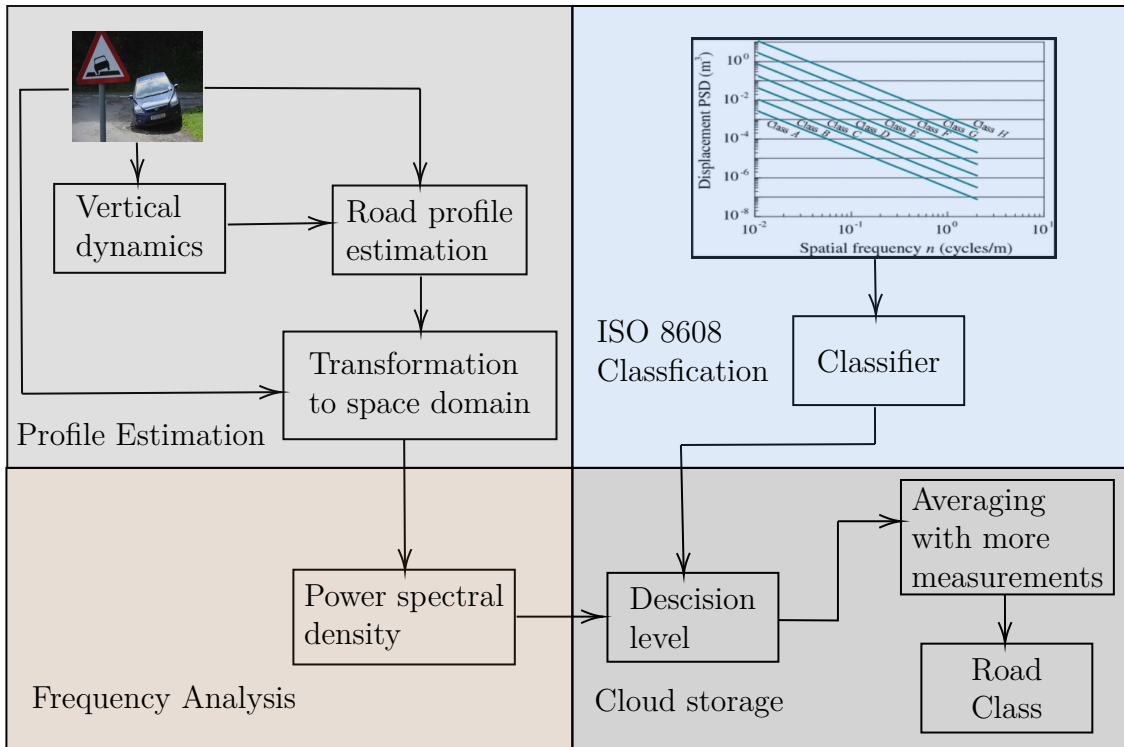
Figure 3.1: Methodolgy

As seen from the figure above the process involves estimation of the road profile and classification obtained from the sensor data of a vehicle with semi-active suspension system

- **Profile Estimation** : To estimate the suspension parameters using $\mathcal{H}_\infty$ observer as discussed in section 2 and thereafter estimate the road profile based on the static equation of the unsprung mass accelerations (2.8).
- **Frequency analysis** : By using the profile estimate in the time domain, Frequency components of the road signals is determined and the corresponding power acquired in each frequency is determined.
- **ISO 8608 Classification** : Classification standard of the type of roads based on power spectral densities. Given an idea about the road surface irregularity.

The quarter car model represented as state space representation is used for the estimation of road profile. The best way to understand the performance of a model for respective inputs is through the singular value of frequency response of the system. The linear plant model dynamics with road and damper force as inputs can be can be seen in figure 3.2.
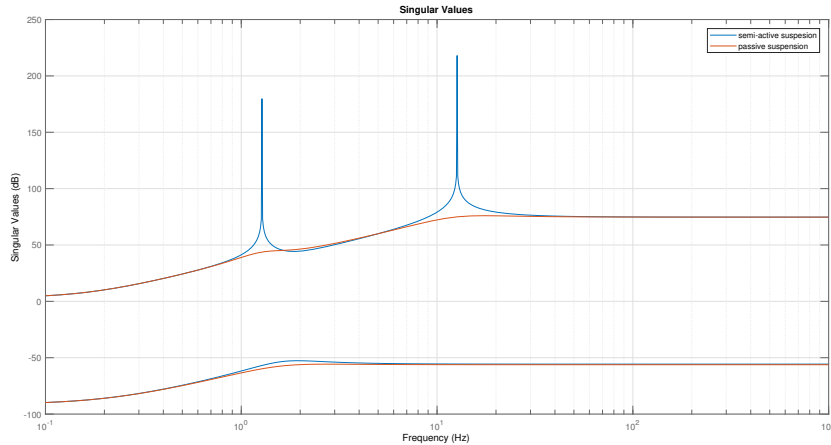

Figure 3.2: System dynamic of semi active suspension with passive suspension system

Figure 3.2 also shows the difference between the semi-active suspension and the passive suspension system. Since the damper force is considered as a continuously changing input to the model and not included in the state space dynamic model we can observe the invariant peaks at two frequencies. The figure shows two plots obtained from the two inputs. The plot with higher singular values is due to the road input on body displacement and the other is due to the damper force input on the body displacement. The transfer function between damper force input to the body displacement and velocity has imaginary zeros with resonance at 73.84rad/s (12Hz), this frequency is called the wheel hop frequency. And the transfer function between the suspension deflection and damper force produces imaginary zero with resonance at 20.82rad/s(3Hz) is called the rattle space frequency.

Hence in a semi-active suspension system it is assumed to have an actuator connected between unsprung and sprung mass to control the suspension over complete bandwidth of the two frequencies, to provide a better ride performance. In case of the passive suspension system, since there is no assumption of controlled damper force between the two masses, the peaks at the two frequencies are highly damped.

The overall estimation model of a closed loop structure with an observer as a feedback and control inputs are estimated states as outputs is then built.
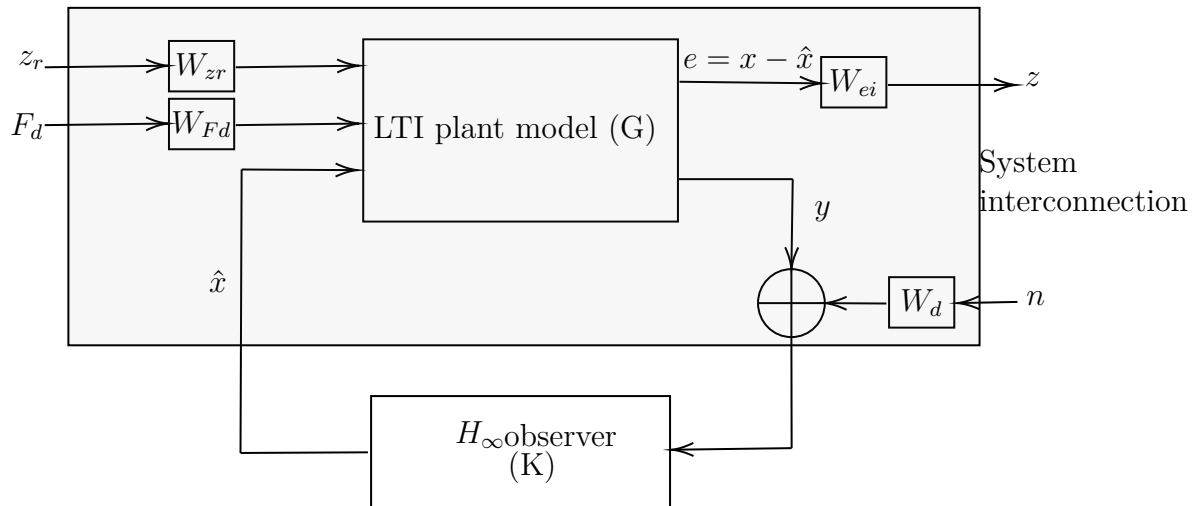
Figure 3.3: $\mathcal{H}_\infty$ Estimation method

Optimized observer is synthesized in order to make the $\mathcal{H}_\infty$ norm as low as possible. To obtain this condition three weighting functions are added to the plant for loop shaping as shown in figure 3.3. A loop-shaping technique to design performance filters in the optimization setting is used for the observer design. This thesis does not deal with robustness issues with a controller design and focuses more on $\mathcal{H}_\infty$ optimization to the frequency dependant loop-shaping state observers. The optimized state observer estimates the suspension parameters as control inputs fed back to the plant model which in turn minimizes the error dynamics and reducing the effect of the measurement noise.

The filter specifications used in the design of $\mathcal{H}_\infty$ observer is explained below. Finding an appropriate weighting function is a crucial step in the robust control design which requires few trials.

From fig 3.3 the weighting matrix denoted by W_{zr} is the loop shaping transfer function responsible to shape the irregularities of the road in the frequency band of interest. This is shown in 3.4. The road variability consists of slow changing profiles and high frequency irregularities, a relevant part of the road spectrum is a suitable choice to affect the dynamics of the vehicle. The slow variability in the road profile less than 0.01 cycles/m (0.3Hz) or wavelength above 100 m and similarly the high frequency irregularities greater that 5 cycles/m (30Hz) or wavelength below 0.5m are filtered out since it is difficult to measure high frequencies with the sensors used and very low frequencies do not affect the vehicle dynamics, hence they are not included in the spectrum. The region covered with boundary in the red color shows the region of interest.
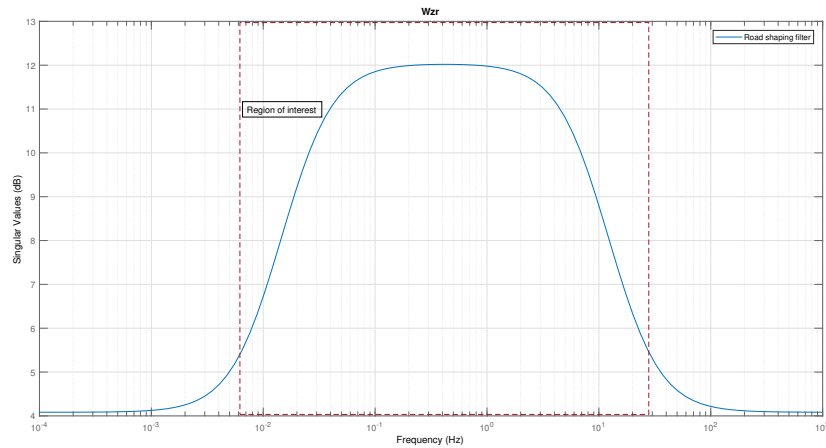
Figure 3.4: Road shaping filter

The actuator CCD model is an approximation of the behaviour the physical system which accounts for varying displacements and modelling errors. There exists a nominal behaviour with frequency dependant amount of uncertainty. At lower frequency around 0.1Hz a 40% uncertainty of the nominal model is applied and at frequency greater than 3Hz the uncertainty is greater than 100% of the nominal value. An input multiplicative uncertainty model is developed as a weighting to the actuator which can be seen in figure 3.5. The nominal model is represented with black color in the right half of the figure. The uncertainties shown are respective to that nominal model. These input uncertainties are included in the filter design since factors such as change in current reading due to external parameters such as temperatures or small displacement errors in the deflection velocity brings changes in the damper force. Therefore to account for this changes an input multiplicative uncertainty is considered for the actuator model.
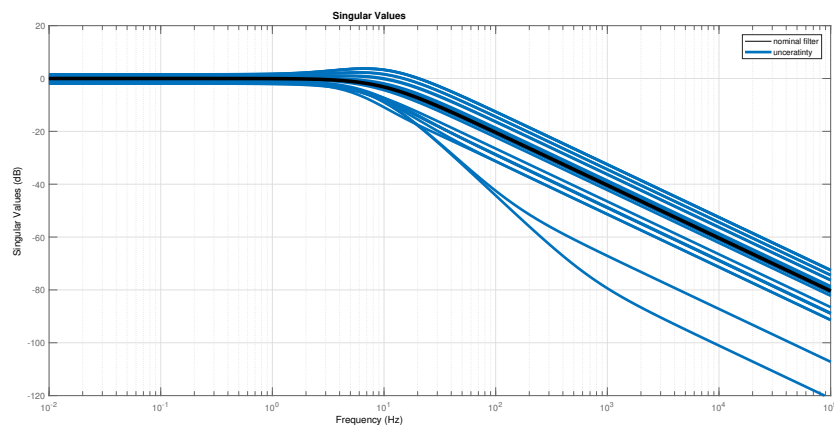

Figure 3.5: Actuator uncertainty model

Another weighting from the figure 3.3 represents the performance weightings. It is used in the minimization of the estimation error in the frequency region of the

suspension operation. To achieve a desired performance of noise reduction it is necessary to satisfy the inequality condition $||W_{ei}(I+GK)^{-1}||_\infty < 1$. The singular values of the sensitivity function $(I+GK)^{-1}$ must lie below the inverse of the weighting function $(\frac{1}{W_{ei}})$ for all frequencies as shown in figure 3.6. Hence a precisely tuned performance weighting has to be chosen
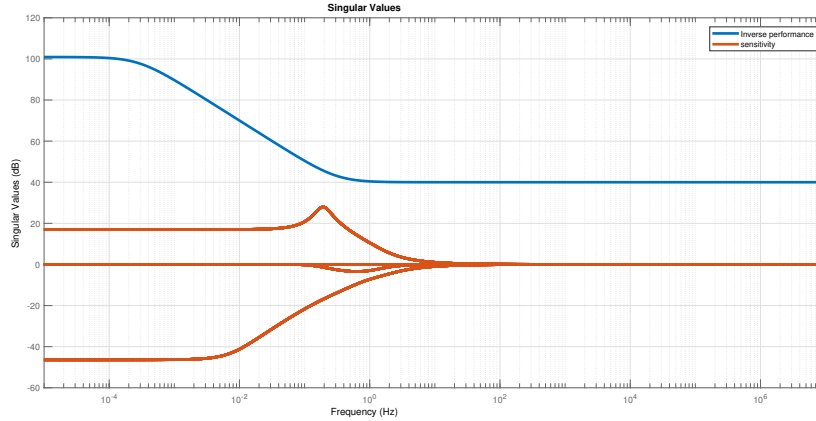
Figure 3.6: Choice of performance weightings against the sensitivity

In general case, the measurement noise is a complementary sensitivity function from a classical closed loop transfer equation 3.1 which describes that less weightage is given to the noise signals which are generally present in the higher frequencies of the sensor signals.

$$y = \underbrace{(I+GK)^{-1}GK}_{T}\,r + \underbrace{(I+GK)^{-1}}_{S}\,G_d d - \underbrace{(I+GK)^{-1}GK}_{T}\,n \qquad (3.1)$$

Figure 3.7: Weighted noise measurements

All these filters are used in support of loop shaping techniques to operate the system in the frequency region of interest. Whereas, for lower frequencies which includes

slower dynamics of the road it might account to small drift from an accelerometer sensor. The structure of the open loop system is then interconnected with all the weightings. By taking into account the the performance outputs and weights given

$$\begin{bmatrix} z \\ y \end{bmatrix} = P \begin{bmatrix} d_1 \\ d_2 \\ u \end{bmatrix} \tag{3.2}$$
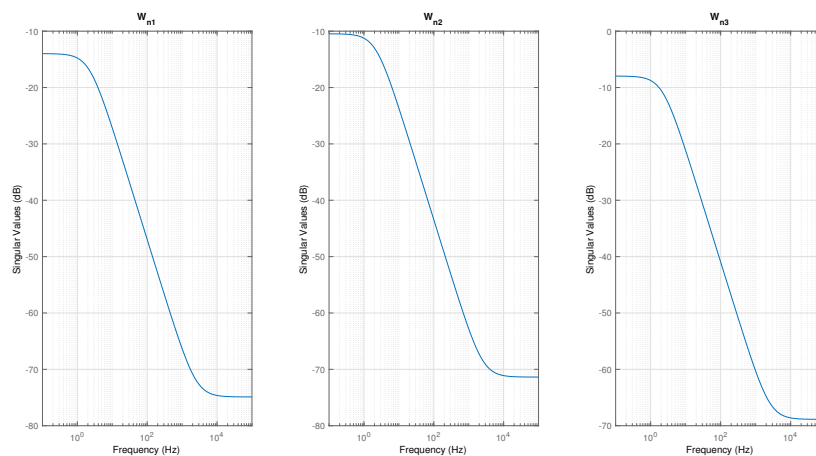
Here d_1 is an input to the weighting matrices $W_{in} = diag(W_{Fd}, W_{zr})$, d_2 is the disturbance input to W_d and $u = \hat{x}$ the control input.

By using the equations for inputs and outputs i.e the performance output and the measurement output

$$\begin{aligned} z &= W_{ei}GW_{in}d_1 - W_{ei}u \\ y &= GW_{in}d_1 + W_d d_2 \end{aligned} \tag{3.3}$$

the interconnected block P will take the form

$$\begin{bmatrix} z \\ y \end{bmatrix} = \begin{bmatrix} W_{ei}GW_{in} & 0 & -W_{ei} \\ GW_{in} & W_d & 0 \end{bmatrix} \begin{bmatrix} d_1 \\ d_2 \\ u \end{bmatrix} \tag{3.4}$$

where,

$$P = \begin{bmatrix} W_{ei}GW_{in} & 0 & -W_{ei} \\ GW_{in} & W_d & 0 \end{bmatrix} \tag{3.5}$$

The system interconnected block P is then used in the $\mathcal{H}_\infty$ synthesis with measurements as inputs and estimated states as the number of outputs System interconnection can also be done by using *sysic* command from the MATLAB.

3.2 Power Spectral Density

Road profile data $z_r(t)$ is converted to frequency domain by using Fourier transformation to determine the frequency components of the signal. By knowing the vehicle velocity equivalent road profile $z_r(x)$ is determined in spatial domain and spatial angular frequency domain can also be determined, since space domain is the best way to classify the roads according to ISO 8608 classification.

By using a Matlab function "*pwelch*" it is possible to determine the power spectral density of the spatial domain signal directly. This uses a similar method as explained in section 2.4 The *pwelch*() method uses a moving window technique where FFT is computed and then PSD is computed as average of FFT's over all windows. This method is dependant on three parameters.

- **Window length (N)** : The convention of choosing the window size N is set to the power of 2 greater than the length of the signal. But this procedure would make it less efficient and faster implementation of the FFT. If N is less than

the length of the signal then FFT will utilize only N samples to estimate the PSD. An effective utilization of the window size is to be chosen such that the number of windows used over the data is effective. This will help in obtaining a smooth PSD. Frequency resolution (distance between two frequency points) is another factor that should be taken care of such that important frequency components are not lost.

A suitable window size is chosen in this thesis considering 2000 samples per second of signals of varying length. By using a window function such as Hamming window it is possible to have very less side-lobes and makes it better option for frequency selective analysis.

- **Overlap percentage** : The change in the overlap percentage varies the effects of noise in the signal. Lower overlap percentage with 0% increases the overall noise in the PSD, and with increase in the overlap percentage to 50% increases the number of windows and helps in the averaging of the effects of noise. Increasing it further to 100%, the correlation between the windows samples increases, thus averaging brings no effect on the noise.
  Therefore 50% noise is taken into consideration

- **Number of FFT points** : The number of FFT points chosen is equal to the length of the window

3.2.1   ISO 8608 Classification

ISO is a worldwide federation of national standards designated to form standards of rules for the specified work. The committee responsible for the document related to road classification is *"Mechanical vibration, shock and condition monitoring"*. The road profile classification is done by standards mentioned in the ISO 8608 [25]. The power spectral density of a road profile is defined by

$$G_q(n) = G_q(n_0) \left(\frac{n}{n_0} \right)^{-w} \tag{3.6}$$

n is the spatial frequency and n_0 is the reference spatial frequency of $0.1m^{-1}$ and $G_q(n)$ is the power spectral density at spatial frequency n. The reference PSD $G_q(n_0)$ determines the differences in the road classes, where smallest value shows better roads and greater values the bad roads. w represents the waviness of the road with greater values of w representing higher amplitudes and lower frequency and smaller values of w representing higher frequency and lower amplitudes. But ISO 8608 uses w=2 as the waviness.
The ISO road level definition is given by

Road Class	$G_q(n_0)10^{-6}m^3$
A	16
B	64
C	256
D	1024
E	4096
F	16,384

Table 3.1: Road level definition by ISO

The representation of all the classes from A to F with values given in table 3.1 can be seen in the figure 3.8. The road profile estimates will be described by the PSD of its vertical displacement. As seen in the figure 3.8 the PSD is in m^3 versus the spatial frequency in cycles/m are on the logarithmic scale. The below figure also represents the fitted PSD which describes the region around the type of road.

Since the spatial frequency range is important for vehicle dynamics analysis, the range for which is chosen between $n\epsilon[0.01\ 4]cycles/m$.

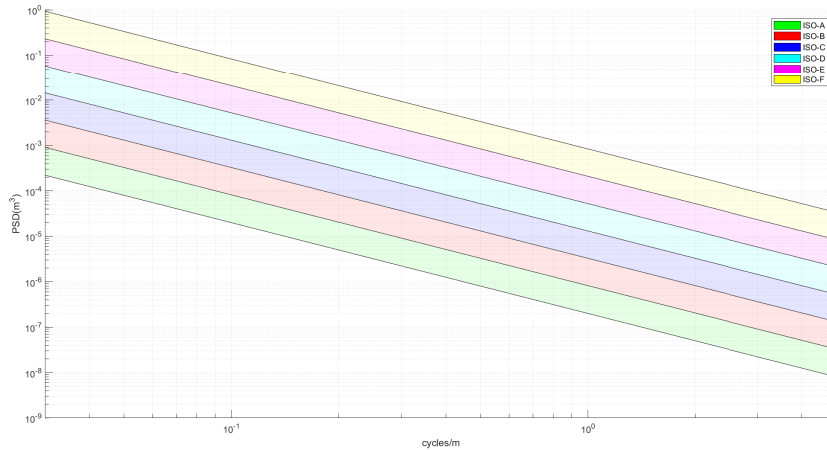**Figure 3.8:** Classification of roads from A to F

For the vehicle driven at a velocity of $\mathcal{V}\ ms^{-1}$ the spatial PSD can be transformed into time domain PSD as in equation 3.7

$$G_q(f) = \frac{1}{v}G_q(n) = G_q(n_0)n_0^2\frac{\mathcal{V}}{f^2} \tag{3.7}$$

where f is the frequency in Hz. The relation between the excitation energy of the PSD coefficient $G_q(n_0)n_0^2$ and the vehicle velocity can be seen in 3.9. The figure shows that the increase in vehicle velocity increases the the roughness coefficient. Therefore, the vehicle velocity is directly proportional to the roughness coefficient.
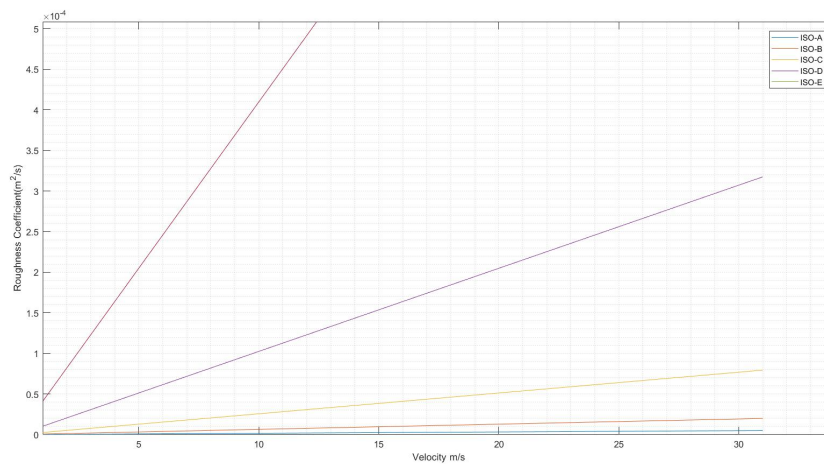
Figure 3.9: Roughness coefficient vs velocity

The PSD of the road profile is not always a straight line, since the frequency component of the irregularity differ in different octave bands. Therefore, the spatial frequency range is divided into six segments for easier classification. The figure 3.10 shows the mean and limit values of $G_d(n)$ for different octave bands. This figure is the PSD representation divided throughout the center frequencies by the ISO standards. Here only segments for valid spatial frequency range between 0.00625 cycles/m to 4 cycles/m.

Road class	Mean and limits $G_d(n_c)$ 10^{-6} m³	Octave centre spatial frequency, n_c cycles/m									
		0,007 8	0,015 6	0,031 2	0,062 5	0,125	0,25	0,5	1	2	4
A	Mean	2 621	655	164	41,0	10,2	2,56	0,64	0,16	0,04	0,010
	Upper	5 243	1 311	328	81,9	20,5	5,12	1,28	0,32	0,08	0,020
B	Lower	5 243	1 311	328	81,9	20,5	5,12	1,28	0,32	0,08	0,020
	Mean	10 486	2 621	655	163,8	41,0	10,24	2,56	0,64	0,16	0,040
	Upper	20 972	5 243	1 311	327,7	81,9	20,48	5,12	1,28	0,32	0,080
C	Lower	20 972	5 243	1 311	327,7	81,9	20,48	5,12	1,28	0,32	0,080
	Mean	41 943	10 486	2 621	655,4	163,8	40,96	10,24	2,56	0,64	0,160
	Upper	83 886	20 972	5 243	1 310,7	327,7	81,92	20,48	5,12	1,28	0,320
D	Lower	83 886	20 972	5 243	1 310,7	327,7	81,92	20,48	5,12	1,28	0,320
	Mean	167 772	41 943	10 486	2 621,4	655,4	163,84	40,96	10,24	2,56	0,640
	Upper	335 544	83 886	20 972	5 242,9	1 310,7	327,68	81,92	20,48	5,12	1,280
E	Lower	335 544	83 886	20 972	5 242,9	1 310,7	327,68	81,92	20,48	5,12	1,280
	Mean	671 089	167 772	41 943	10 485,8	2 621,4	655,36	163,84	40,96	10,24	2,560
	Upper	1 342 177	335 544	83 886	20 971,5	5 242,9	1 310,72	327,68	81,92	20,48	5,120
F	Lower	1 342 177	335 544	83 886	20 971,5	5 242,9	1 310,72	327,68	81,92	20,48	5,120
	Mean	2 684 354	671 089	167 772	41 943,0	10 485,8	2 621,44	655,36	163,84	40,96	10,240
	Upper	5 368 709	1 342 177	335 544	83 886,1	20 971,5	5 242,88	1 310,72	327,68	81,92	20,480

Figure 3.10: PSD of different classes of roads divided through center frequencies by ISO 8608 [25]

4

Results

The results of the estimation and the classification for the roads are presented in this section. Results are divided into simulation results i.e testing it on the Car-Maker and experimental results (sensor data collected by driving the vehicle on test tracks). High frequency roads and low frequency roads are both part of the experimental result structure. In the experimental data, the speed of the vehicle is almost maintained as a constant. Later a classification study is done comparing the roads with the ISO standard roads. The effect of these on the primary ride and secondary ride is also studied and definition of how it helps in the damping control is also analyzed.

The available tools and sensors used during this thesis are limited to existing vehicle sensors. The effect of this limitation is studied and the results are discussed.

4.1 Estimation Results

4.1.1 CarMaker

CarMaker is a software tool which consists of entire vehicle dynamics comprising of suspension, vertical, lateral, longitudinal and tire dynamics. Hence the obtained results will be considered to be behaving very close to the CarMaker data. Therefore, the roads are considered from this software for testing.

The road models from CarMaker is used in order to test the estimation results. Several road conditions are included in order to determine the classification on the type of the road to be determined. High frequency disturbance roads and roads having very slow change in the topography i.e low frequency disturbance are some of the roads used for the classification.

Whilst having the road model built, there are certain parameters needed to be set in the CarMaker.

- Maneuvering : The speed at which the vehicle moves on the road profile is set here. To account offset of the vehicle position is also set here.
- Road bumps : The road bumps are set in the parameters section. Beams or waves is chosen to test in order to have single or multiple bumps. Another option used is a CRG file i,e a built in model of certain roads which replicate the real road scenario is also chosen.
- Vehicle Parameters : Mass of the vehicle, suspension parameters are needed to be set.
- Sensors : For obtaining the measurements from the maneuver of the vehicle,

respective sensors such as body accelerometers and position sensors placed in the vehicle are used.

4.1.2 Estimation of suspension parameters

The suspension parameters comprising of the states used to determine the road profile is estimated here. CarMaker software tool as explained above is used to verify and analyze the estimated parameters of the suspension from the observations. The observer is built by considering measurements used from the vehicle sensor data. The mounted senors provide information about the suspension behaviour in real time which is useful in validation and verification of the estimates. In order to first validate the observer, measurements are chosen from the linear model and tested, the results for which can be seen in figure 4.1. Different bumps and symmetrical/unsymmetrical roads are part of the result. The car in the simulation is run at a different speeds, On the wavy road (a) the vehicle speed is 50kmph, Unsymmetrical waves(b) at 35kmph, Road roughness(c) at 30kmph and on Belgian road(d) at 70kmph. The measurements sprung deflection and velocity and the sprung mass accelerations are chosen from the linear model and given as an input to the observer. The outputs are the state estimates sprung mass displacements $\hat{z}_s$, sprung mass velocity $\dot{\hat{z}}_s$, unsprung mass displacement $\hat{z}_u s$, and unsprung mass velocity $\dot{\hat{z}}_{us}$. The linear model outputs are shown in blue and the estimates are in red.

(a) Waves

(b) Unsymmetrical Waves
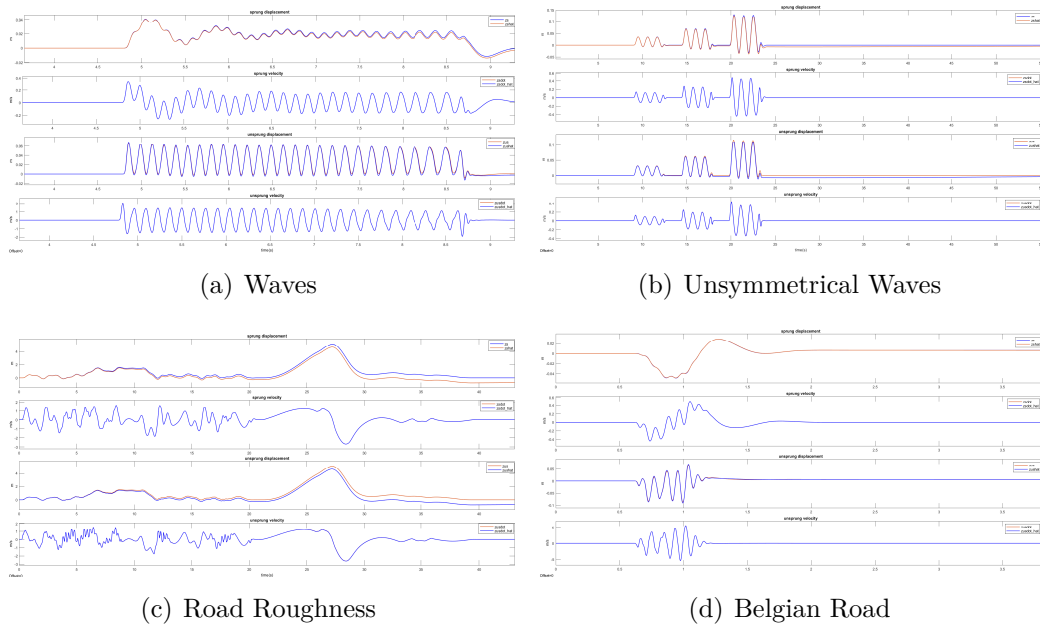
(c) Road Roughness

(d) Belgian Road

Figure 4.1: Estimates for CarMaker demo road surfaces with linear model

The same observer is tested with the non-linear model from the CarMaker, the results for which can be seen below. The results show the states matches precisely with that of the CarMaker sensor data. These are further used in estimation of the road profile. Figure 4.2 shows the similar roads tested with the linear model. The vehicle speed is the same as used for verification with the linear model.
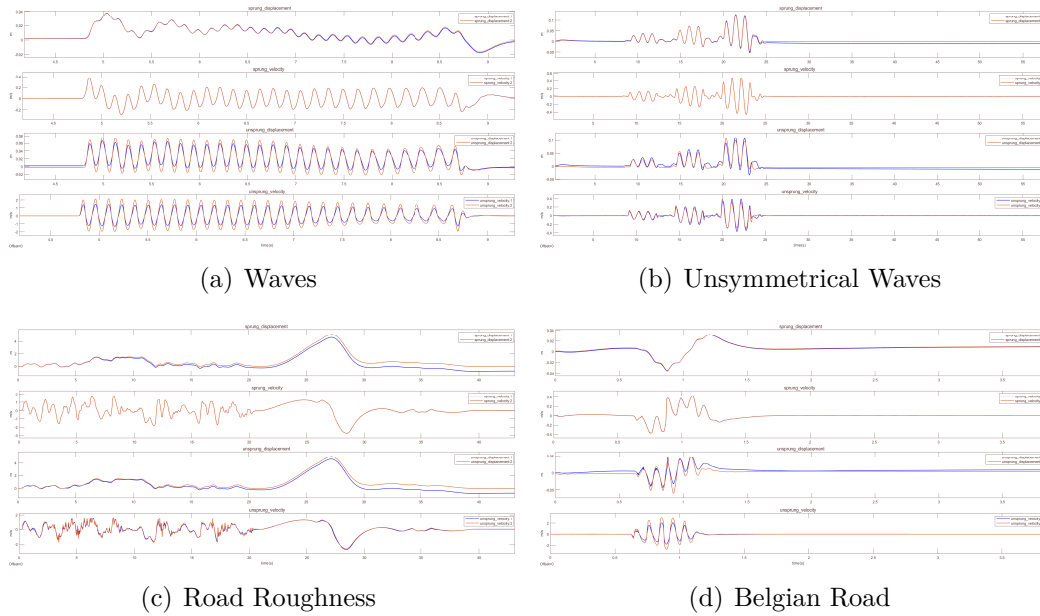
(a) Waves

(b) Unsymmetrical Waves

(c) Road Roughness

(d) Belgian Road

Figure 4.2: Estimates for CarMaker demo road surfaces with nonlinear model

Two roads are further chosen to compare and analyze the road estimate and the frequency components of the profile. The roads chosen are the best example to study the effects of the road irregularities affecting the control of the damper as a result of the ride quality. The two roads are given the names Road A and road B. They have symmetrical and unsymmetrical wavelengths of profile irregularities which could be distinguished by the frequency components.
Road A has track width of 3m and driven on the center lane with no offset. The length of entire road is around 550m and the vehicle is driven at a speed of 65 kmph.
Road B has a track width of 3m and driven on center lane without any offset. The length of the road is around 300m and speed of the vehicle is 70 kmph. Figures 4.3 and 4.4 shows the state estimates of Road A and Road B in comparison with actual state values from the CarMaker.
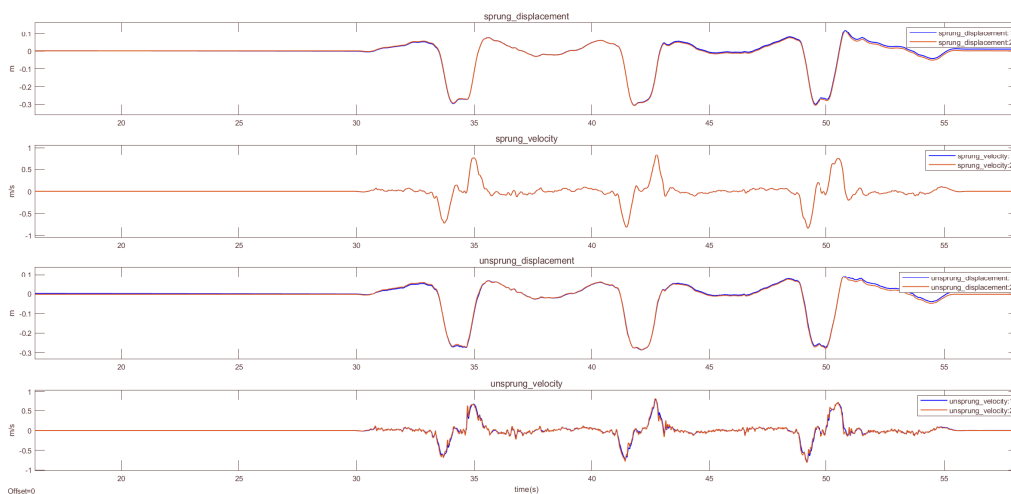

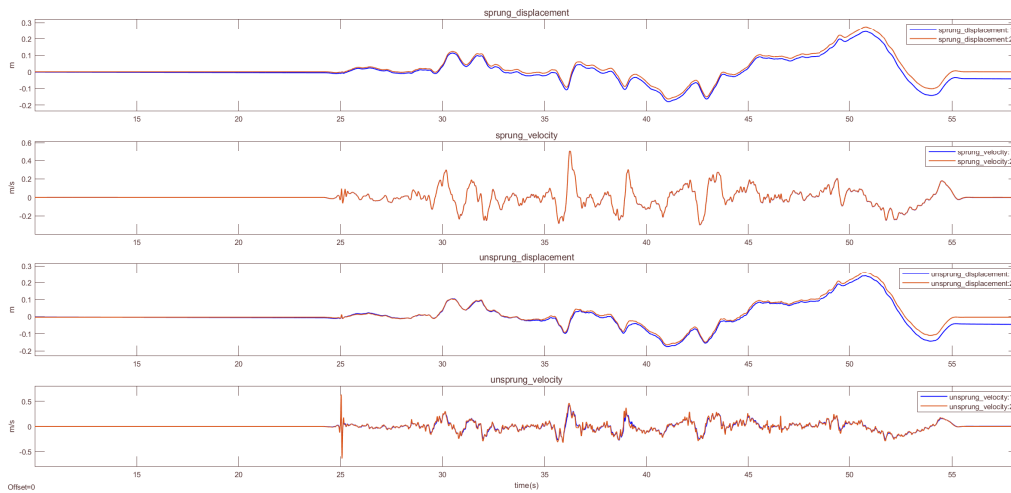**Figure 4.3:** Suspension parameters estimate for road A

Figure 4.4: Suspension parameters estimate for road B

Further these estimates are used to construct the road profile, which is presented in the next section.

4.1.3 Road Estimation Model

The road estimation is done based on the estimations obtained from the observer. The profile estimate obtained is a proximity of the real road profile. Since the unsprung mass accelerometer is not a part of the observed vehicle measurement, It is determined from the estimated states by taking the derivative of the unsprung velocity and then filtered to obtain the data only from the range of interest.
Equation 2.8 is used to estimate the road profile. The estimated unsprung mass accelerations $\hat{\ddot{z}}_{us}$ for the two roads A and B is shown in figure 4.5 and 4.6.
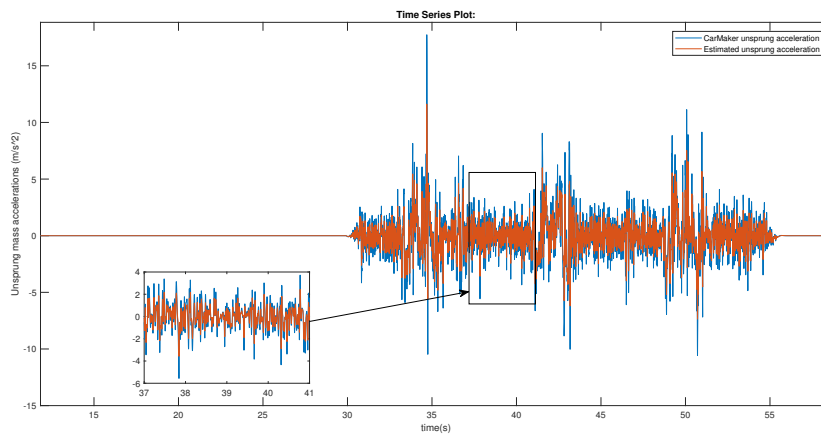
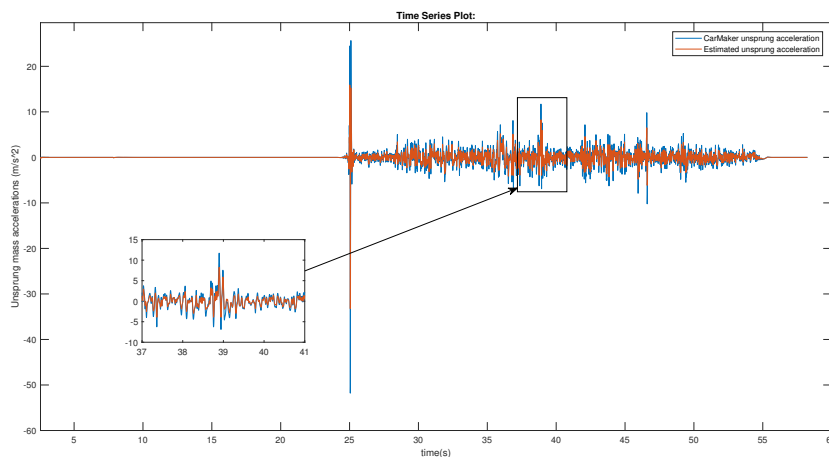**Figure 4.5:** Unsprung mass acceleration for road A

Figure 4.6: Unsprung mass acceleration for road B

The road profile $\hat{z}_r(t)$ shown is in the time domain, therefore, with the speed of the vehicle it is possible to determine an equivalent road profile $\hat{z}_r(x)$ as a function of the road length x. The estimate is then passed through a moving average filter which acts as a simple low pass(FIR) filter. A suitable filter length is chosen such that any important modulations in the profile data is not affected. Road estimate for road A is shown in 4.7 and road B is shown in 4.8
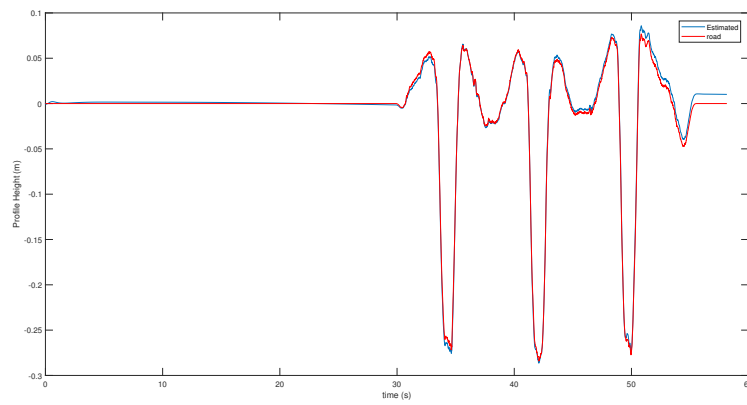
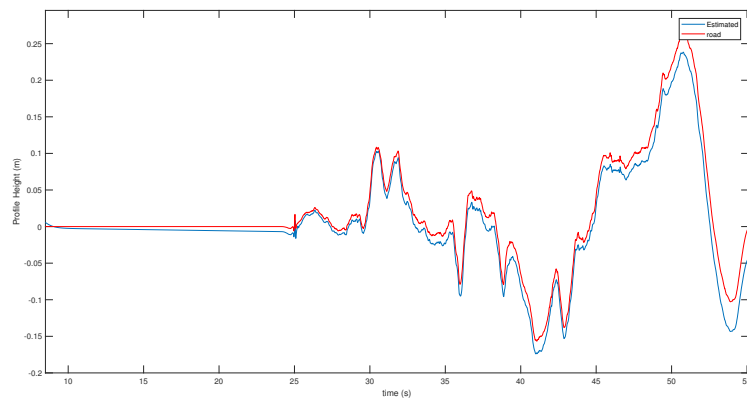**Figure 4.7:** Road profile estimate for road A

Figure 4.8: Road profile estimate for road B

4.2 Frequency Analysis and Power spectrum density

Frequency analysis is carried out for the road estimates in the previous subsection 4.1. It is necessary to study the frequency components of these roads as they build the notion of any prolonged disturbances from the road, which could be plausible harm to the vehicle or human body. They even provide information for the control of the vehicle suspension on a specific length of the road, helping in improving the ride quality and the handling of the car. Human body is another such complex structure with different organs resonating at different frequencies. Hence knowing the frequency components of the road is vital aspect of vehicle dynamics.
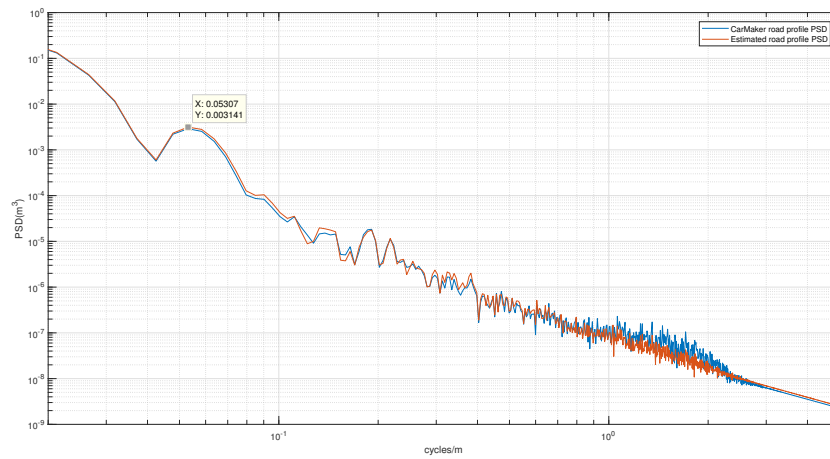

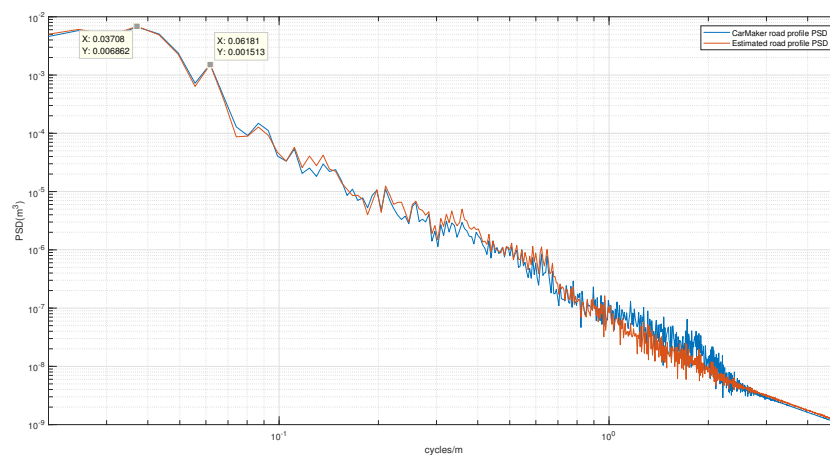**Figure 4.9:** PSD comparison for Road A

Figure 4.10: PSD comparison for Road B

Since the scope of the thesis remains to classify these roads based on its condition,

power spectral density is the best way to define the road's spatial frequency component because it is independent of the velocity of the vehicle. The PSD for Road A shown in figure 4.9 clearly represents a low frequency disturbance in the road with a peak around 0.053 cycles/m, with the vehicle moving at a velocity of 75 kmph and the PSD for road B is shown in 4.10 with multiple frequency disturbances with peaks at 0.03 cycles/m and 0.06 cycles/m. The figures also show the comparison between the real road profile from the CarMaker road sensor data and the estimated road profile. It is clear to see the similarities between the estimated spectral densities.

The vehicles travelling on a single lane won't always be travelling in the same width of the track. For example if a lane has a width of 3m, the vehicle might travel with some offset of 0.5m, 1m or greater. A test is done to check the similar circumstance. Road A is considered for this. Figure 4.11 shows the vehicle travelled on the same track but having some offsets in the track position. The offset of 1m is set for the car position. Although the PSD of the shown road profile almost remains the same. The power spectral density of road with an offset shown is for the left wheel, similar experiment is carried out with an observer at the right wheel.
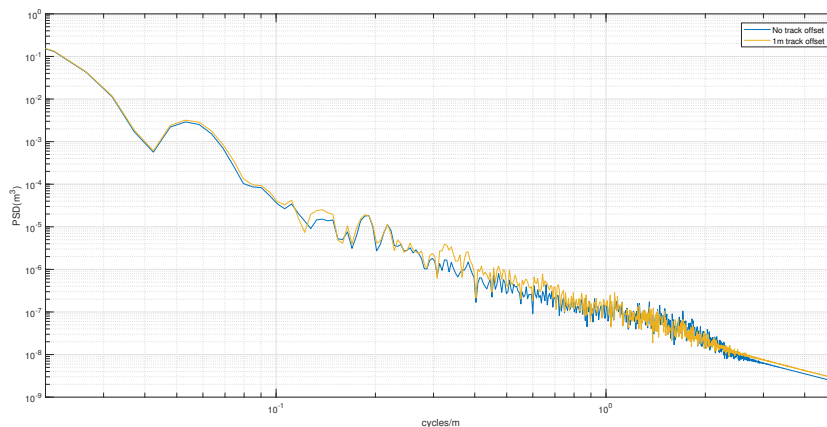

Figure 4.11: PSD comparison for offsets

The spatial frequency is used in the ISO standard classification of the roads and the importance of representing the spectral density in spatial frequency can be seen from figure 4.12. Road A is considered in this case as well. The vehicle is driven on the same track at different speeds i.e 48kmph, 75kmph, 90kmph, 120kmph and 150kmph. Since moving at different speeds on the same road profiles would have different time domain frequency disturbance, whereas the spatial frequency would show the same peak for all varying velocities which is easy to understand and represent. Although there arises few differences when vehicle is moving at higher speeds which is due to the suspension settings on the vehicle. Comparison with the ISO standards is shown in the appendix.
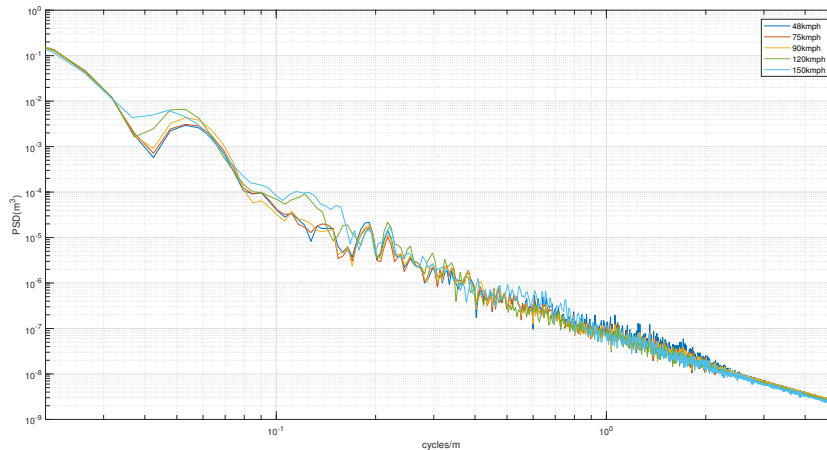
Figure 4.12: PSD comparison at varying speeds

4.3   Experimental results

Section 4.2 explains about the examples considering the measurements form the Car-Maker sensor data. This would still consider an ideal case in real world with very less uncertainties and disturbances. Therefore, real world measurements are collected from the sensors placed on vehicle and driven on test tracks. Similar observer model is used for estimation of the states using these sensor measurements with more uncertainties and disturbances present in them. The measurements sprung mass accelerations $\ddot{z}_s$ and suspension deflection z_{def} from the sensors are sampled at 2000Hz and an offline estimation is done in Simulink. These measurements sprung mass acceleration is low pass filtered at 30Hz to include the region of interest for the dynamics. This filtered data in turn removes additional noise affecting the estimation. In turn the deflecting velocity of the suspension which is differentiated and filtered from the suspension deflection data is another measurement passed as an input to the observer.

Different examples of various roads are provided below. These are the roads from the experimental test tracks. The suspension estimates and the respective road profiles are shown. The unsprung mass acceleration used in determining the road estimates are obtained from the suspension estimates.

Figure 4.13 and 4.14 represents the state and road estimates respectively for road with manholes on the left side of the track present at a distance of 40m approximately. It shows that the amplitude is quite small which makes the sprung mass movement very negligible compared to the unsprung mass movement.
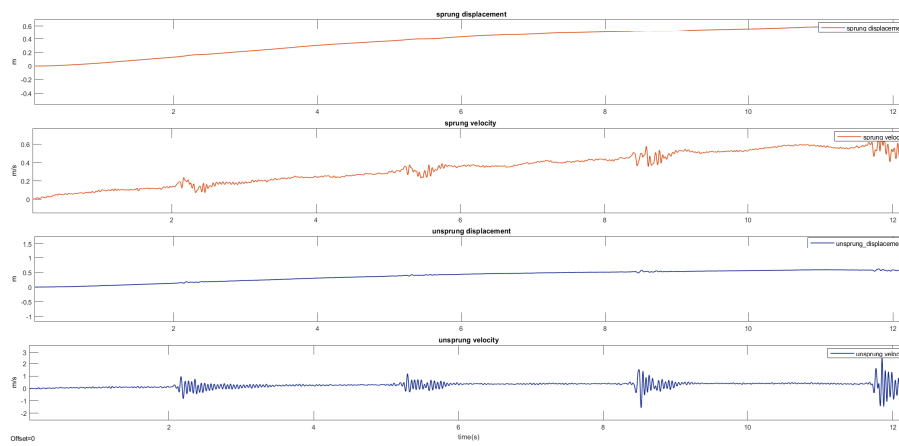

Figure 4.13: Suspension parameter estimate for manhole road

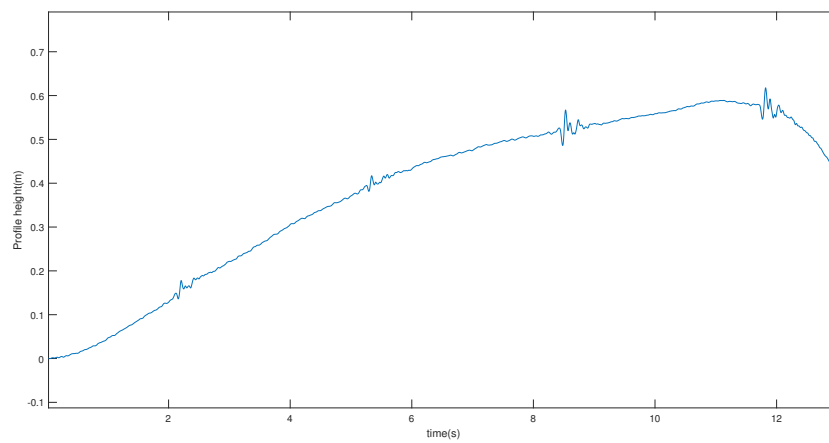The road estimates shows very such small dips representing profile irregularity.

Figure 4.14: Road estimate for manhole road

Figure 4.15 and 4.16 represents the state and road estimates respectively for road with roll excitation on left side of the track. It shows a constant dip at an equidistant distance. These roads create discomfort when the vehicle body rolls to the left. Since the measurements used are limited and the vehicle roll is not plotted here.
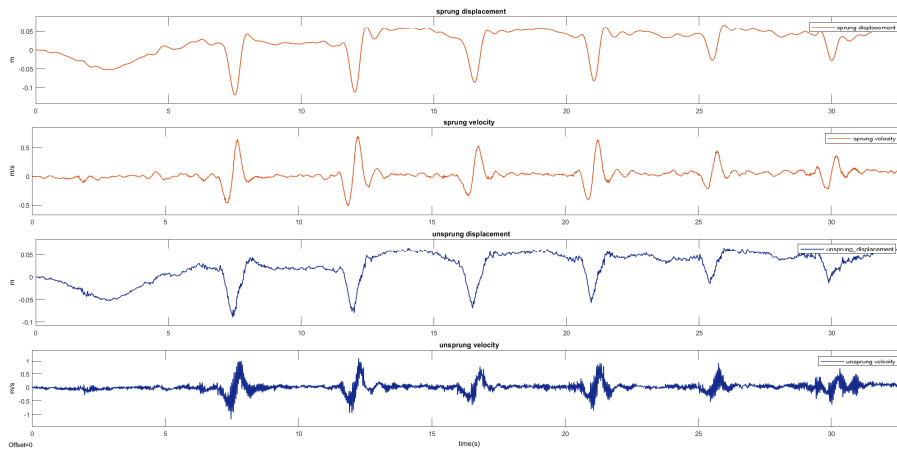

Figure 4.15: Suspension parameter estimate for roll excitation on Front left wheel

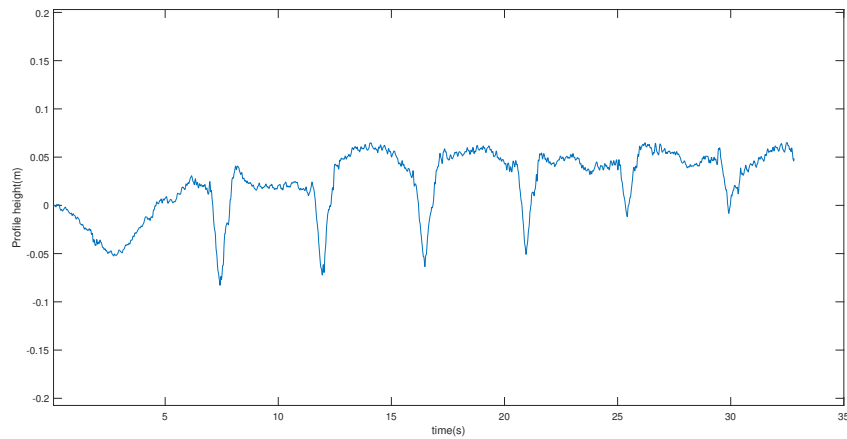The road estimates shows the dips from the left wheel representing profile irregularity.

Figure 4.16: Road estimate for roll excitation on front left wheel

Figure 4.17 and 4.18 represents the state and road estimates respectively for road with low dips at equidistant distance. These are the low frequency disturbances affecting the primary rides in vehicle dynamics. These roads are similar to road A of the section 4.2.
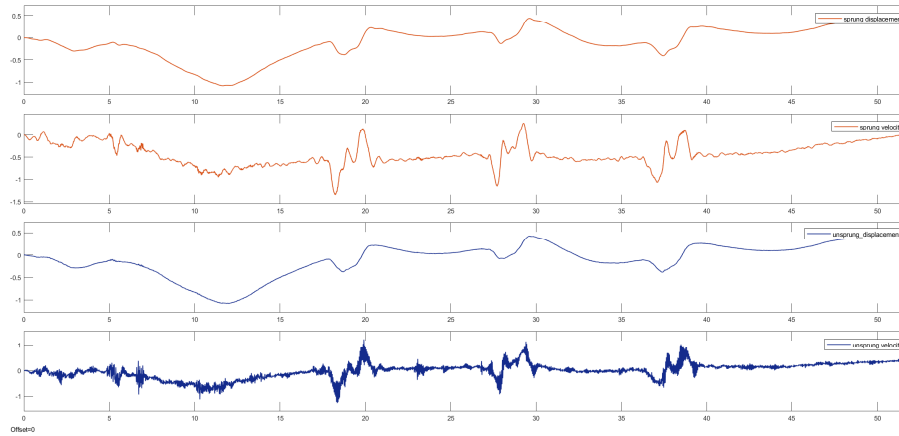

Figure 4.17: Suspension parameter estimate for low frequency road

The road estimates shows the low frequency long dips representing profile irregularity.
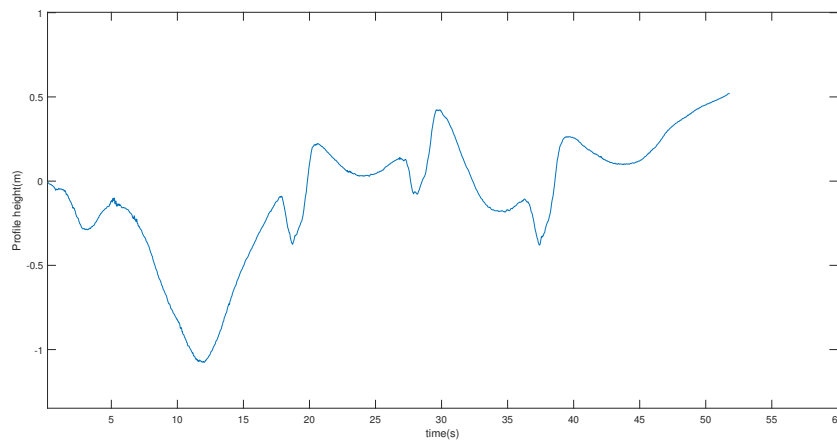

Figure 4.18: Road estimate for low frequency road

Figure 4.19 and 4.20 represents the state and road estimates respectively for road with high frequency disturbances which affects the secondary ride in vehicle dynamics. These roads have unsymmetric wavelengths of road profiles.
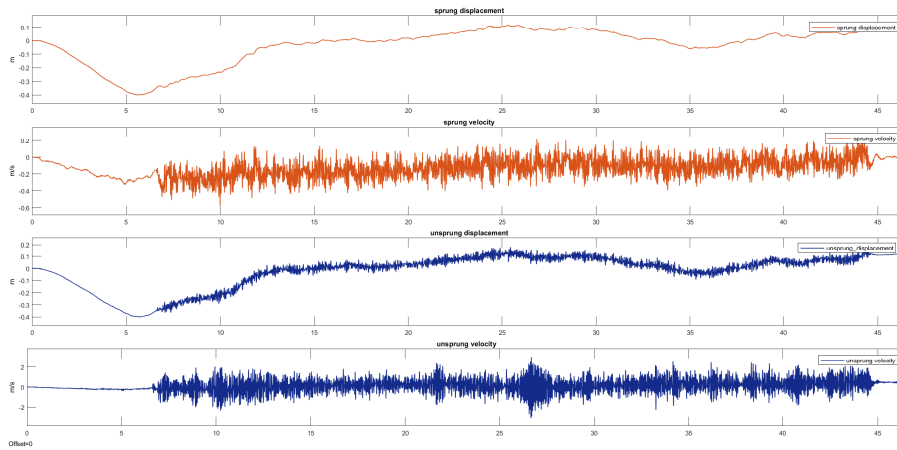

Figure 4.19: Suspension parameter estimate for high frequency road

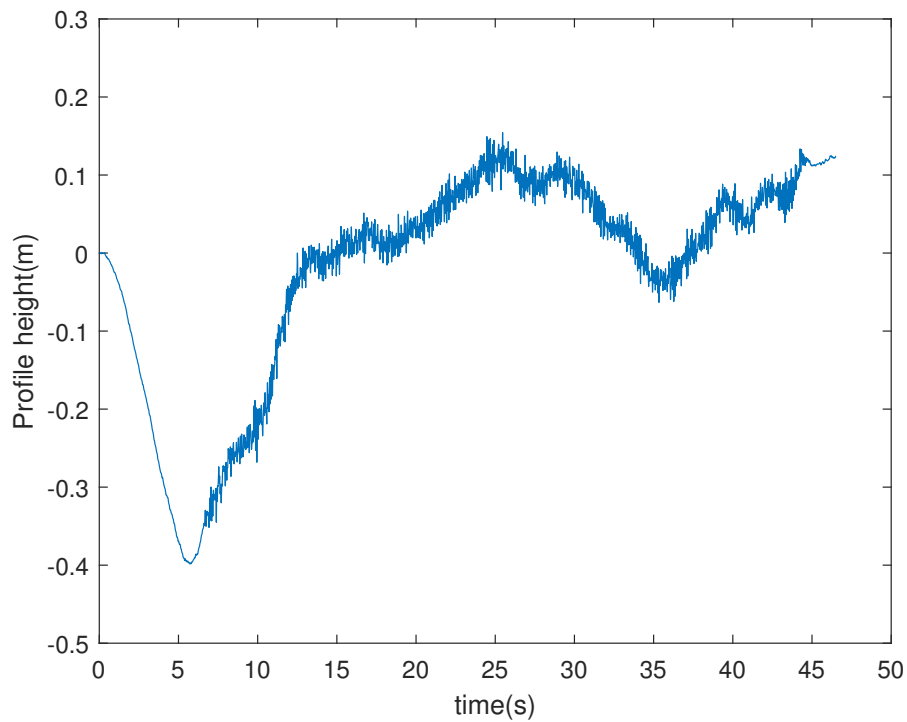The road estimates shows high frequency profile irregularity.

Figure 4.20: Road estimate for high frequency road

4.3.1 Frequency analysis and PSD for Experimental data

Two roads representing low frequency and high frequency disturbance i.e road estimates from figures 4.18 and 4.20 are considered. Frequency components of these two roads can be seen below.
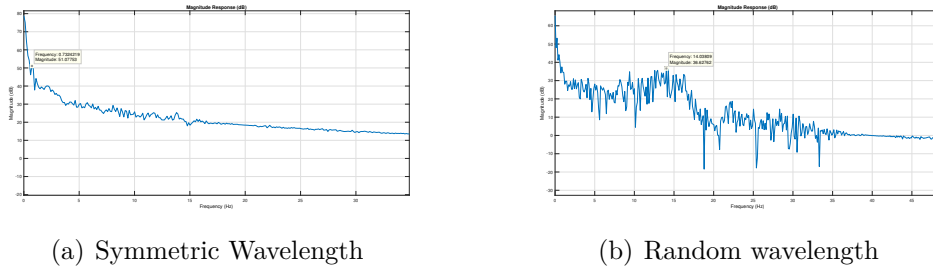

(a) Symmetric Wavelength

(b) Random wavelength

Figure 4.21: Primary and secondary ride roads

As already discussed the power spectral density in spatial domain is the region of interest, further results will feature comparison of the spectral density in units of wavenumber. One road to easily compare the data from CarMaker and experimental data is the low frequency road. Figure 4.22 show the PSD of the roads, although at higher frequencies few uncertainties and different damping controls might be few reasons of small differences. The peak obtained from CarMaker is at 0.058 cycles/m and the peak obtained from the experimental data is at 0.06 cycles/m which shows not much difference between them. This would be an ideal case for the classification of road.

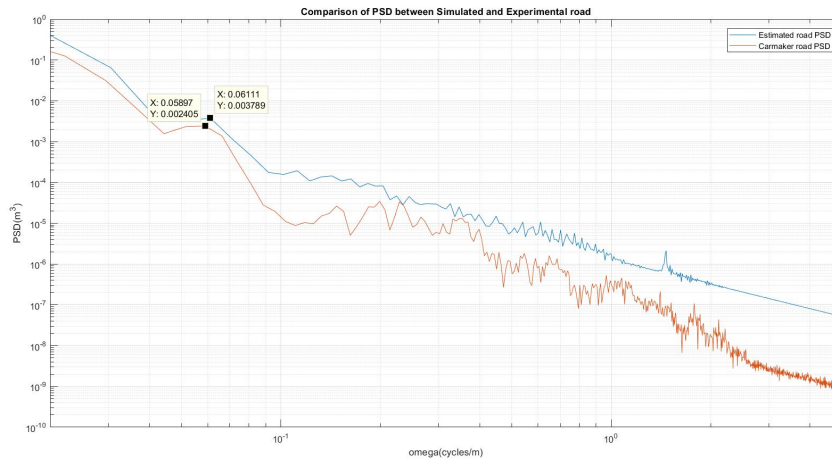**Figure 4.22:** Comparison between CarMaker PSD estimate and experimental PSD estimate

In order to verify power spectral density of the experimental data for high frequency road, the car is driven on the same track twice first at 60kmph and then 70kmph, the result of which can be seen in the 4.23. The figure shows the PSD for the same road width for left and right wheel. The result shows that the power spectral densities of

the same road matches hence it could be useful for classification of the type of the road.
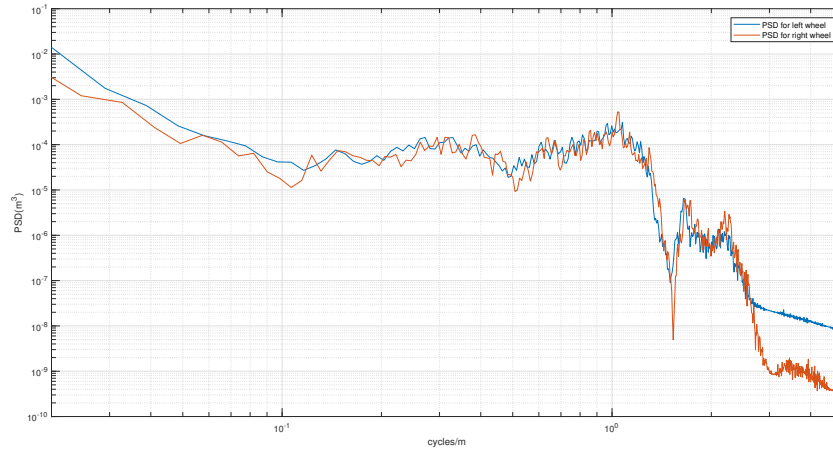

Figure 4.23: PSD comparison when driven on same road back and forth

4.3.2 ISO Classification

The power spectral densities of the road estimates is compared to ISO standards as explained in the section 3.2.1. This makes it easier to classify the roads at different spatial frequency and provide an idea for the control of the dampers. Figure 4.24 shows the PSD for low frequency roads on the fitted PSD classes of the ISO standards. The low frequency road is the experimental road estimate represented in figure 4.18. The peak frequency in spatial domain is around 0.06 cycles/m or 0.74Hz with the vehicle travelling at 15.5 m/s.
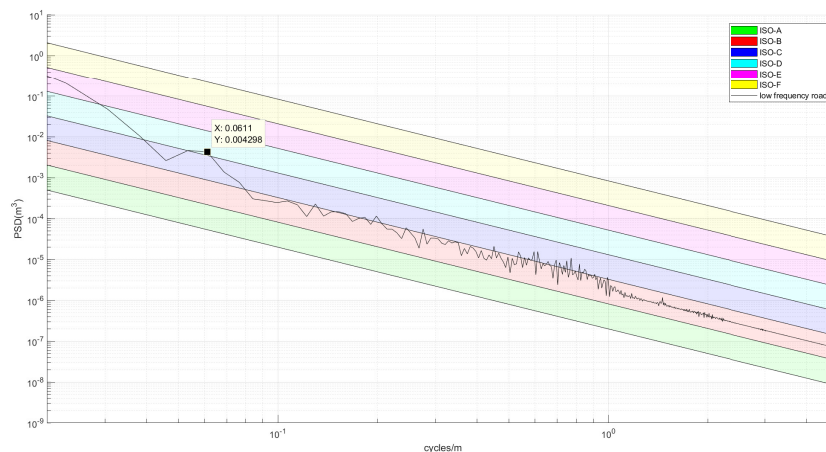

Figure 4.24: Displacement PSD of low frequency road

In figure 4.25(a) shows type of classes for all points of spectral density in spatial frequency range and 4.25(b) shows the peak frequency at a particular central frequency

of in the spatial frequency octave bands. The central frequencies for division into frequency segments is given in figure 3.10. The classification based on the central frequency will provide clear information for setting the damper control for primary and the secondary ride. As it can be seen the the central frequency 0.06 cycles/m shows the peak for the low frequency disturbance.

(a) PSD for specified frequencies	(b) PSD only for central frequencies

Figure 4.25: Primary and secondary ride roads

The parameters for such classification can be seen in table 4.1. The standard of the road is said to be ISO-C class at lower frequencies.

RMS speed	15.5 m/s
Peak Frequency	0.74 Hz
Spatial frequency	0.06 cycles/m
Road Class	ISO-C

Table 4.1: Parameters of low frequency road classification

Similarly, figure A.1 shows the PSD of high frequency road on the fitted ISO standards, The high frequency road is the experimental road one shown in figure A.1. The peak frequency is at 1.075 cycles/m or 14.03 Hz. The velocity of the vehicle moving is at 14 m/s.

Figure 4.26: Displacement PSD of high frequency road

In figure 4.27(a) shows type of classes for all points of spectral density and 4.27(b) shows the peak frequency at a particular central frequency of in the spatial frequency octave bands. The parameters of such classification can be seen in table 4.2. It can be seen that the peak can be seen for a central frequency of around 1 cycle/m.

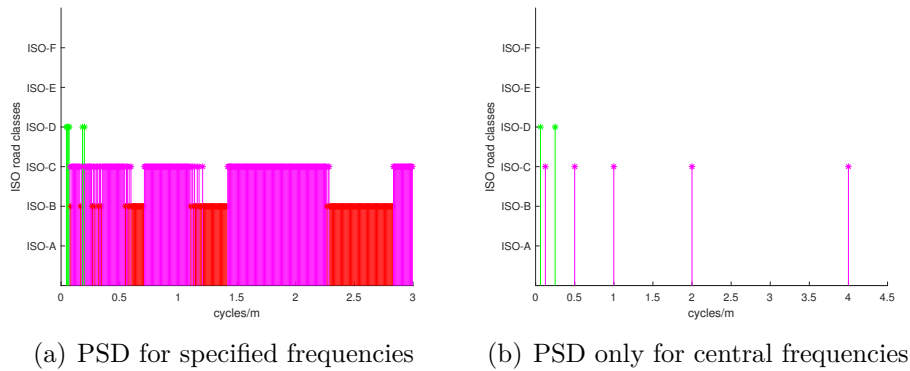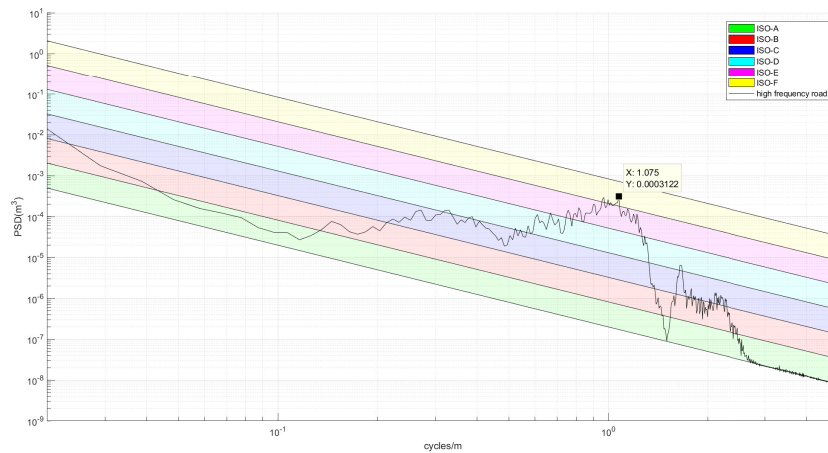(a) Symmetric Wavelength

(b) Random wavelength
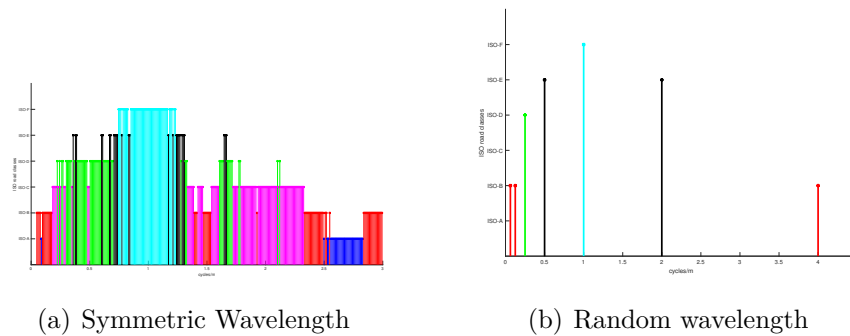
Figure 4.27: Primary and secondary ride roads

The parameters for this classification can be seen in table 4.2. The standard of the road is said to be ISO-F class at higher frequencies.

RMS speed	14 m/s
Peak Frequency	14.03 Hz
Spatial frequency	1.075 cycles/m
Road Class	ISO-F

Table 4.2: Parameters of high frequency road classification

Similarly, classification could be done for all the estimated road profile based on the PSD as given by the ISO standardization. Meanwhile the ISO standardized classification considers the waviness of any type of road to be fixed at 2. A classification

algorithm to include different waviness for different roads is included in the future scope.

4.3.3 Decision for Damper tuning for Primary and Secondary ride

The operation condition of a vehicle is subjected to many vibrations in the vehicle body caused by many things at different frequencies. The vibration that creates discomfort to passengers can be distinguished by different ways as seen in figure 4.28
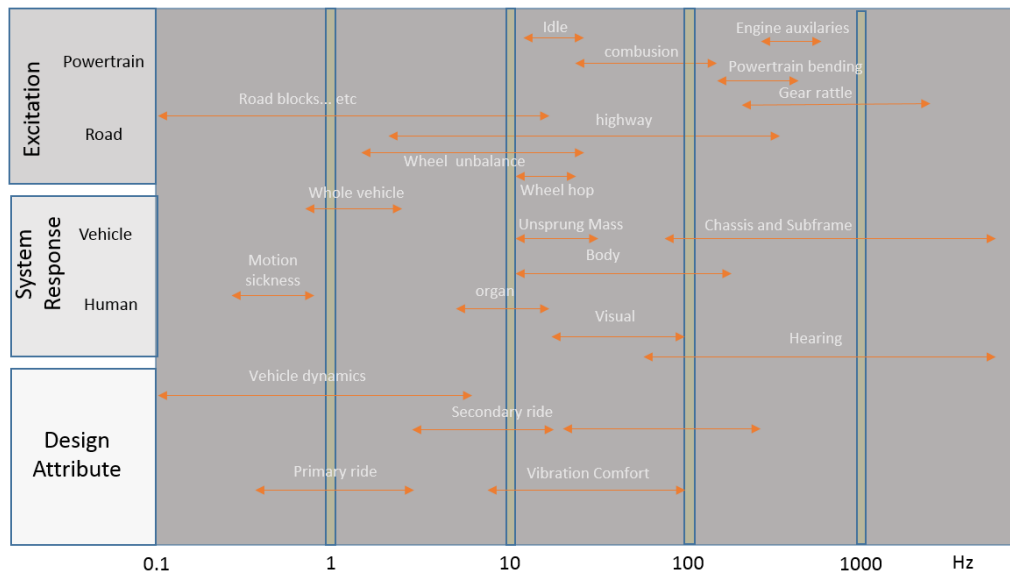

Figure 4.28: Maneuvering frequency ranges

In automotive industry the ride behaviour is described by primary and secondary ride. The primary ride would describe the road with bumps having higher amplitudes and lower frequencies. Such topographic variation would be visible to the naked eye whilst driving. Such riding conditions of the road is termed as the primary ride. Which includes suspension movement over undulations related to the bound and rebound of the dampers.

Secondary ride is small irregularities with low amplitudes but higher frequencies Which is slightly difficult to be seen from the moving vehicle. Such irregularities are mainly due to combination of damper and bushing control. The tuning in secondary ride involves the dampers and bushings to work well.

The frequency content of the primary ride is less than 6Hz, with the wavelength greater than the wheel base of the vehicle. These roads mostly have symmetric profile. An example of such road profile can be seen in figure 4.29(a) The frequency component of the secondary ride has medium frequency range around 8Hz and greater. The irregularities in the road profile is continuously varying in large spectrum of wavelengths. This can be seen in figure 4.29(b)
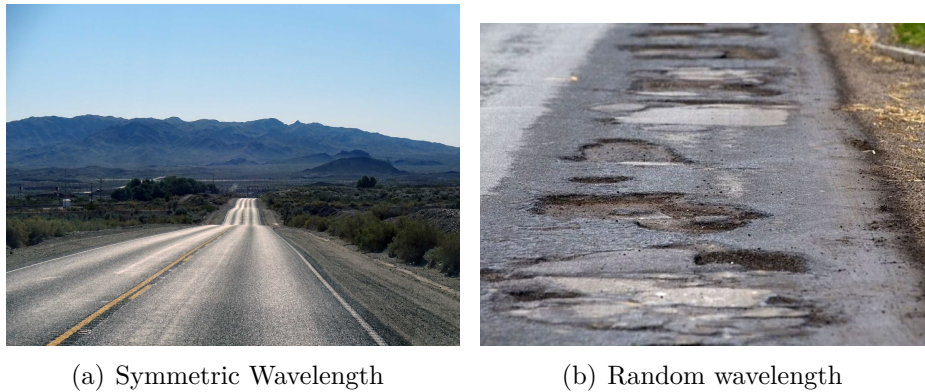
(a) Symmetric Wavelength   (b) Random wavelength

Figure 4.29: Primary and secondary ride roads

Influence of the low frequency and high frequency roads from the results on primary and secondary ride can be

- Low frequency roads in the primary ride must have a suspension damping increased to get better damping at frequencies below 6Hz which eliminates the peak frequencies in that region and improves the ride quality. But with same settings if the vehicle is driven on the high frequency roads then the ride quality is deteriorated causing a slower roll-off and harshness.
- High frequency roads in the secondary ride must have a suspension damping decreased to get better damping at higher frequencies from 8Hz to above eliminating the peak frequencies improve the ride quality. If with same setting the vehicle is driven on low frequencies then it will have a large impact on the passenger.

4.4 Future Scope

- The suspension parameter estimation uses a quarter car model which operates in a lower frequency region where the accelerometer data tends to drift with a very slow varying slope, hence a full car model can be used to build an observer to handle the case of slow varying topographies.
- The estimated states can also be used to the control the damper force.
- Here a classification is done using a continuous time observer model. An online estimation can be done by discretising the model and the observer at a specific sampling rate.
- The ISO classification uses the waviness of the road to be 2 for all sets of road. A different classification standards could be considered for varying sets of waviness of the roads depending on the reference classes of the road.

5
Conclusion

The main objective of this thesis was to to estimate the road profile and classify the road based on the roughness of the road. The first chapter introduced many techniques used in the current market for estimation of the classes of the road and road profile. Response based road profile estimation was the one considered. The second chapter gives insight into the vehicle modeling. The continuous damper in the semi-active suspension model is explained along with a quarter car model of the left wheel suspension model. Road profile estimation model is also defined. The robust observer $\mathcal{H}_\infty$ model is derived for the estimation of the suspension parameters later used to estimate the road profile. The third chapter explains about the method in which the estimation and classification is done. The choice of filter specifications and loop shaping for the robust observer is explained. The ISO standards for classification of the road profile based on power spectral density in the spatial frequency domain is introduced. The last chapter is used to explain the results obtained from the simulations from Carmaker data and the experimental results from the sensor data collected from the measurements run on the test tracks.

Bibliography

[1] DGIP. EU road surfaces: Economic and safety impact of the lack of regular road maintenance, study. *Policy Department Structural and Cohesion Policies*, European Parliament,2014.

[2] S. Gerwens. European Manifesto: Need for road maintenance. Pavement Preservation and Recycling, Summit, 2015.

[3] US department of transportation. Long-term pavement performance program

[4] Z. Zhang, C. Sun, R. Bridgelall, et al. *Application of a machine learning method to evaluate road roughness from connected vehicles.* Journal of Transportation Engineering, Part B: Pavements, 144(4):04018043, 2018. DOI: 10.1061/jpeodx.0000074.

[5] R. Bridgelall, Y. Huang, Z. Zhang, et al. Precision enhancement of pavement roughness localization with connected vehicles. Measurement Science and Technology, 27(2):025012, 2016. DOI: 10.1088/0957-0233/27/2/025012

[6] Y. Qin, M. Dong, F. Zhao, et al. Comprehensive analysis for influence of controllable damper time delay on semi-active suspension control strategies. Journal of Vibration and Acoustics Transactions of ASME, 139(6):031006, 2017. DOI: 10.1115/1.4035700.

[7] K. Mcghee. Automated pavement distress collection techniques. Transportation Research Board, 2004.

[8] H. Imine, Y. Delanne, and N. K. M'sirdi. Road profile input estimation in vehicle dynamics simulation. Vehicle System Dynamics, 44(4):285–303, 2006. DOI:10.1080/00423110500333840.

[9] Acuity AR600/RP: Laser displacement sensor for road profilometry. https://www.Acuitylaser.Com/Docs/Ar600-Road-Profiling.Pdf

[10] M. Ahmed and F. Svaricek. Preview optimal control of vehicle semi-active suspension based on partitioning of chassis acceleration and tire load spectra. Proc. of the Control Conference (ECC), 2014. DOI: 10.1109/ecc.2014.6862615.

[11] Z. Yuan, X. Zhang, S. Liu, et al. Laser line recognition for autonomous road roughness measurement. Proc. of the Cyber Technology in Automation, Control, and Intelligent Systems (Cyber), 2015. DOI: 10.1109/cyber.2015.7287977.

[12] M. Aki, T. Rojanaarpa, K. Nakano, et al. Road surface recognition using laser radar for automatic platooning. IEEE Transactions on Intelligent Transportation Systems, 17(10):2800–2810, 2016. DOI: 10.1109/tits.2016.2528892.

[13] D. Hrovat and W. Tseng. Adaptive active vehicle suspension system. US Patents. 1995.

[14] K. Yi and B. Song. A new adaptive sky-hook control of vehicle semi-active suspensions.Proc. of the Institution of Mechanical Engineers,

Part D: Journal of Automobile Engineering, 213(3):293–303, 1999. DOI: 10.1243/0954407991526874.

[15] H. Imine, Y. Delanne, and N. K. M'sirdi. Road profile input estimation in vehicle dynamics simulation. Vehicle System Dynamics, 44(4):285–303, 2006. DOI: 10.1080/00423110500333840

[16] D. Moustapha, V. Alessandro, A. Charara, et al. Estimation of road profile for vehicle dynamics motion: Experimental validation. American Control Conference, San Francisco, CA, 2011. DOI: 10.1109/acc.2011.5991595.

[17] J. Tudon-Martinez, S. Fergani, O. Sename, et al. Adaptive road profile estimation in semiactive car suspensions. IEEE Transactions on Control Systems Technology, 23(6):2293– 2305, 2015. DOI: 10.1109/tcst.2015.2413937.

[18] S. Wang, S. Kodagoda, L. Shi, et al. Road-terrain classification for land vehicles: Employing an acceleration-based approach. IEEE Vehicular Technology Magazine, 12(3):34–41, 2017. DOI: 10.1109/mvt.2017.2656949.

[19] Y. Qin, Z. Wang, C. Xiang, et al. Speed independent road classification strategy based on vehicle response: Theory and experimental validation. Mechanical Systems and Signal Processing, 117:653–666, 2019. DOI: 10.1016/j.ymssp.2018.07.035.

[20] H. Ngwangwa, P. Heyns, H. Breytenbach, et al. Reconstruction of road defects and road roughness classification using artificial neural networks simulation and vehicle dynamic responses: Application to experimental data. Journal of Terramechanics, 53:1–18, 2014. DOI: 10.1016/j.jterra.2009.08.007.

[21] S. Kang, J. Kim, and G. Kim. Road roughness estimation based on discrete Kalman filter with unknown input. Vehicle System Dynamics, 2018. DOI: 10.1080/00423114.2018.1524151.

[22] Z. Wang, M. Dong, Y. Qin, et al. Road profile estimation for suspension system based on the minimum model error criterion combining with kalman filter. Journal of Vibroengineering, 2017.

[23] G. Xue, H. Zhu, Z. Hu, et al.(2017) Pothole in the dark: Perceiving pothole profiles with participatory urban vehicles. IEEE Transactions on Mobile Computing, 16(5):1408–1419, 2017. DOI: 10.1109/tmc.2016.2597839.2,

[24] A. Gonzalez, E. O'brien and K. Cashell. The use of vehicle acceleration measurements to estimate road roughness. Vehicle System Dynamics, 46(6):483–499, 2008. DOI:10.1080/00423110701485050.6

[25] Mechanical vibration — Road surface profiles — Reporting of measured data, second edition ISO 8608:2016

A
Appendix

The figure represents comparison of the PSD for road profile A at varying velocities with the ISO standard classification. Although most of the classification shows similar classes for the roads at velocities 48kmph, 75kmph and 90kmph but at higher velocities at 120kmph and 150kmph the peak shows road class as Class D, the small uncertainties might be due to the coupling of the front and rear axles.
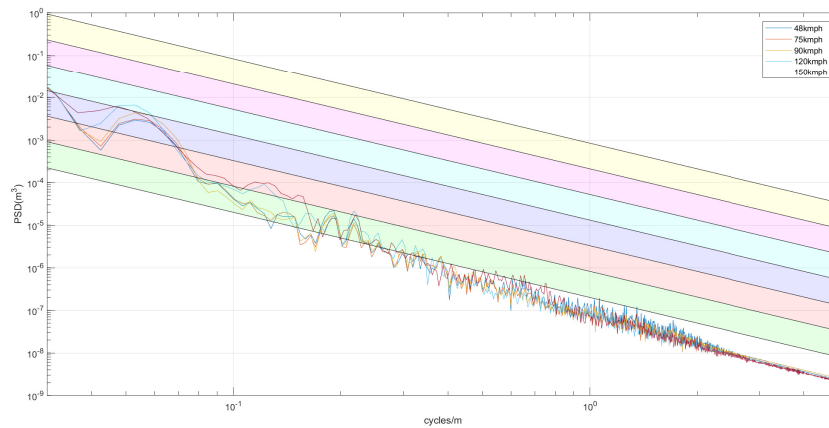

Figure A.1: Comparison of PSD for road profile A at varying velocities with ISO standard classification